ECAP-2016-011

Characterization of a custom designed trigger ASIC (T5TEA) for the Cherenkov Telescope Array

Bachelorarbeit aus der Physik

Vorgelegt von
Jacqueline Catalano
10.08.2016

Erlangen Centre for Astroparticle Physics
Physikalisches Institut II
Friedrich-Alexander-Universität Erlangen-Nürnberg

1. Gutachter: Prof. Dr. Stefan Funk
2. Gutachter: Prof. Dr. Gisela Anton

Abstract

Since the discovery of cosmic rays by Viktor F. Hess in 1912, high energy gamma ray astronomy became more and more advanced. Nowadays, physicists are able to detect radiation up to energies in the range of TeV with large telescopes like H.E.S.S., MAGIC or VERITAS. Sources of very high energy gamma rays are, among others, active galactic nuclei or supernova remnants. The next generation Cherenkov Telescope Array (CTA) is going to be sensitive in the range from a few GeV up to around 300 TeV and will cover an area of about $4\,\mathrm{km}^2$ (in the case of the southern array), which is needed to detect very high energy gamma rays due to their low flux. Cosmic rays initiate air showers in the atmosphere which send out Cherenkov radiation emitted by charged particles faster than the local speed of light. As these Cherenkov flashes are very short in time (few ns), they are hard to detect. Therefore, fast cameras with special read-out electronics need to be developed. In this thesis, one ASIC (application specific integrated circuit) of the newest generation of TARGET, T5TEA, will be presented. T5TEA is a triggering ASIC with 16 input channels and internal generated pedestal (offset) which is able to trigger at low thresholds of a few single photoelectrons (p.e.). It was characterized by its trigger efficiency, behavior with different input pulses, way to vary output pulses and its most important trigger dependent parameters `PMTREF4` and `TRG_THRES`. Also the noise behavior of the channels was studied. Overall, T5TEA shows a better trigger behavior than the former ASIC T5. T5TEA is able to trigger at thresholds of $\sim 4\,\mathrm{mV}$ and with an improvement of the evaluation board it triggers even at $\sim 3\,\mathrm{mV}$.

Contents

1 Introduction **3**
- 1.1 History of high energy gamma ray astronomy . . . 3
- 1.2 Origin of cosmic and gamma rays . . . 4
- 1.3 Cosmic rays in the atmosphere - Cherenkov radiation . . . 4

2 Detection of Cherenkov radiation - CTA **7**
- 2.1 Telescopes . . . 7
- 2.2 Cameras . . . 9

3 TARGET **13**
- 3.1 TARGET ASICs . . . 13
- 3.2 Characterization of T5TEA . . . 14
  - 3.2.1 Transfer function . . . 16
  - 3.2.2 Trigger efficiency . . . 20
  - 3.2.3 Pulse widths . . . 23
  - 3.2.4 `PMTREF4` versus `TRG_THRES` measurement . . . 26
  - 3.2.5 Noise versus threshold measurement . . . 28

4 Summary and outlook **30**

A Appendix **32**
- A.1 Trigger rate vs threshold measurement . . . 32
- A.2 Transfer function measurement . . . 33
  - A.2.1 External measurement . . . 33
  - A.2.2 Internal measurement - TC transfer function . . . 33
- A.3 Trigger efficiency measurement . . . 34
  - A.3.1 Trigger efficiency - 50 Ω . . . 34
  - A.3.2 Trigger efficiency - 410 Ω . . . 36
  - A.3.3 Parameters . . . 38
- A.4 Threshold versus width measurement . . . 39
- A.5 Noise versus threshold measurement . . . 40

References **42**

Acknowledgements/Danksagung **43**

1 Introduction

1.1 History of high energy gamma ray astronomy

From the beginning of mankind, astronomy was an interesting and fascinating topic and became one of the first sciences. Nowadays, we are able to detect very high energy (VHE) radiation in the range of tens of Tera electron-Volt (TeV) [4] which is likely caused by cosmic rays (CRs).
Cosmic rays were first discovered by Viktor F. Hess in 1912 who made manned balloon flights to investigate the ionization of the atmosphere with increasing height. Hess and Kolhörster found that the ionization is raising with increasing height and so the source of the radiation must be located outside the Earth's atmosphere. Later, in 1929, Skobeltsyn investigated β-rays from radioactive decays in a cloud chamber but at the same time he made the first records of tracks generated by CRs (see Figure 1).

Figure 1: First record of a detected CR track in 1929 by Skobeltsyn. The black and white arrows point to the particle track [21].

Bothe and Kolhörster studied the cosmic radiation in more detail to figure out if it consists of high energy (HE) γ-rays or charged particles. Everything indicated that the components of the radiation are charged particles.
Showers of electrons and positrons generated by cosmic rays interacting with the apparatus were detected in a few more cloud chambers experiments. Until 1953, there were discoveries of a few new particles including muons (μ), kaons (K^0, K^+, K^-) and the lambda particle (Λ). Moreover, special "nuclear" emulsions were introduced that make the tracks of charged particles visible. The charged pions (π^+, π^-) decaying into electrons or positrons and neutrinos or anti-neutrinos, which are not directly detectable, the Ξ and the Σ particle were also found until 1953 with such emulsions. This lead to the fact that CRs are at least detected as secondary or higher order charged particles produced by VHE cosmic rays interacting with other particles [21].

1.2 Origin of cosmic and gamma rays

Supernova remnants might be one of the main sources of cosmic rays that compose of protons, electrons and ions interacting with the interstellar medium [8].
Surrounding nebulae of pulsars are also a source of high energy particles. In this scenario, the creation of HE particles flows is caused by rotating magnetic fields [2]. An example for such a nebula is Vela X where a very high energy peak of around 14 TeV was found in the spectral energy distribution (SED) [7].
Representing one third of all known γ-ray emitters in the VHE range, active galactic nuclei[1] (AGN) are another example of these enormous emitters [24], e.g. Mkn 501 emits radiation up to 20 TeV [25].
Moreover, physicists assume that another source of γ-rays could be Dark Matter annihilation [10].
Mergers of two neutron stars or a neutron star and a black hole are assumed to generate so-called gamma ray bursts (GRB) (short lived, $< 2\,\mathrm{s}$) [3], known as "the most powerful explosions in the Universe" [10], which are in the GeV energy range [17]. The long lived ones ($> 2\,\mathrm{s}$) are located in star forming regions of galaxies and are produced by supernovae [13].
Such high energetic radiation can be emitted if the interaction of leptons is non-thermal, e.g. caused by inverse Compton-scattering and synchrotron emission [24], with a neutral pion decaying in two gamma rays or maybe due to dark matter annihilation. The only radiation produced by thermal processes, the so-called blackbody radiation[2], that has such a high energy is the one of the Big Bang [10].

1.3 Cosmic rays in the atmosphere - Cherenkov radiation

When primary hadrons enter the upper atmosphere, they produce a nucleonic air shower as shown in Figure 2. As it can be seen, the hadrons decay predominantly into neutral and charged pions. Then, another decay takes place but this time the neutral and charged pions are involved, which eventually decay into two photons, initiating an electromagnetic cascade (see Figure 3), and in the case of charged pions into other particles like muons. The muons also end up in electromagnetic cascades by decaying into electrons (or positrons) and neutrinos.
Another component of the mentioned particle shower are secondary nuclei which will be ionized and thus lose energy. Additionally, it has to be taken into account that this process depends on the amount of matter that the HE particles have to pass.

[1] Active galactic nuclei are super-massive black holes ($M_{BH} > 10^6\ M_{Sun}$) in the central region of a galaxy [24].

[2] Blackbody radiation is an isotropic and unpolarized radiation [24] that reflects the temperature of the body [10].

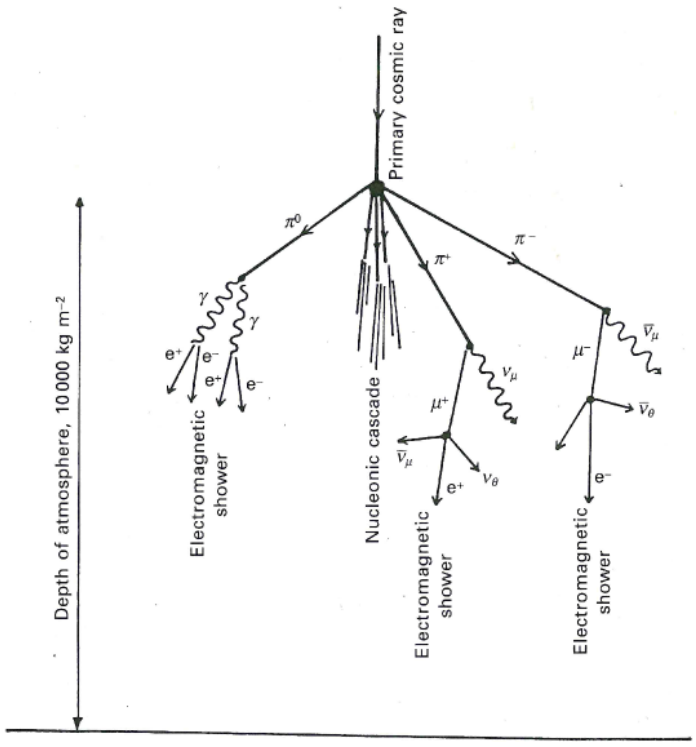

Figure 2: Nucleonic shower initiated by a primary cosmic ray [21].

Electrons and positrons entering the atmosphere or generated by primary gamma rays produce as mentioned before an electromagnetic shower by emitting bremsstrahlung and generating e^-e^+-pairs by pair production (see also Figure 3). These air showers will be detected in form of Cherenkov light with telescopes like H.E.S.S.

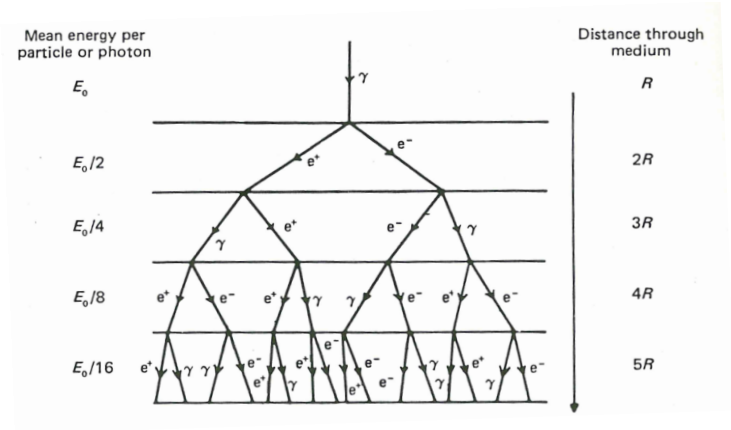

Figure 3: Electromagnetic shower initiated for example by a photon with proper energy [21].

The described electrons and positrons can have velocities greater than the local speed of light in the surrounding medium ($v = \frac{c}{n}$ with n being the refractive index of the medium). When this happens, so-called Cherenkov radiation is emitted as bluish light in the optical range, see for example Figure 4.

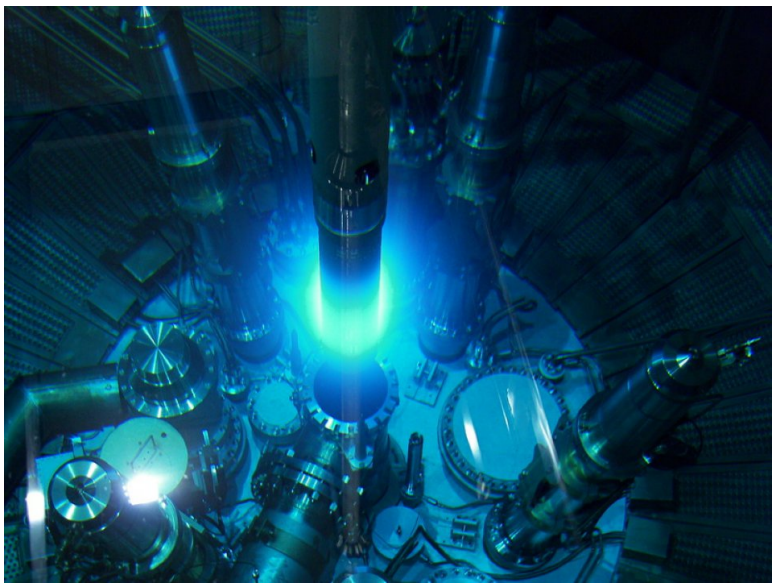

Figure 4: Emitted Cherenkov radiation in water (n=1.33) at the FRM II reactor in Garching, Bavaria [22].

The particles emit the Cherenkov radiation in form of a cone (see Figure 5), which widens with velocity and refractive index.

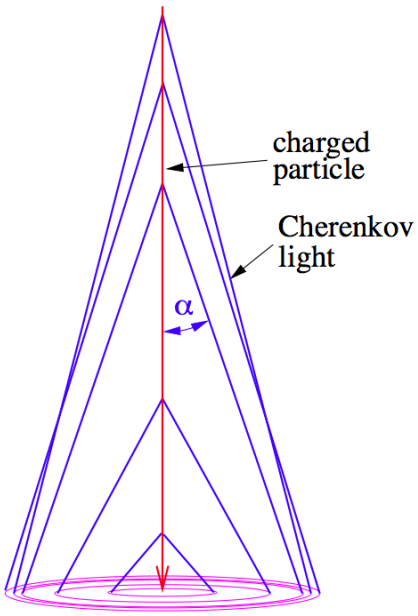

Figure 5: Emitted Cherenkov cone with increasing opening angle α in downwards direction [18].

2 Detection of Cherenkov radiation - CTA

For the detection of Cherenkov radiation, ground-based telescopes like H.E.S.S. or MAGIC are needed. Moreover, a large detection area is favorable because VHE fluxes are low and the emission of Cherenkov light is cone-like (see Figure 6), which causes a circle of roughly 250 m in diameter on the ground for an almost vertically emitted shower [10].

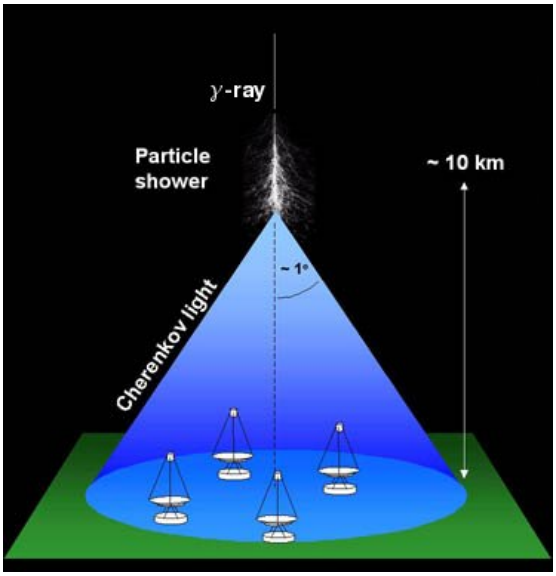

Figure 6: Emitted Cherenkov cone [28].

Therefore, an array of telescopes is the best chance to detect Cherenkov light from high energetic γ-rays.
With an improvement in sensitivity and angular resolution with respect to the already existing Cherenkov telescopes like H.E.S.S., MAGIC or VERITAS, the next-generation Cherenkov Telescope Array (CTA) will propably have an array area of $\sim 4\,\mathrm{km}^2$ on the southern site (Paranal, Chile) and $\sim 0.4\,\mathrm{km}^2$ on the northern site (La Palma, Spain). Arrays on both hemispheres give the opportunity to cover the whole sky for observations.
The array in the North will consist of four large-sized telescopes (LSTs, 23 m diameter) and 15 medium-sized telescopes (MSTs, 12 m diameter). Four LSTs, 25 MSTs and additionally 70 small-sized telescopes (SSTs, 4 m diameter) will perform measurements on the southern hemisphere [14]. The proposed layouts for assembling the telescopes in the North and South can be found in Figure 7a and Figure 7b.

2.1 Telescopes

With telescopes different in size and mirror area, there can be carried out measurements in various energy bands.
Beginning with a few tens of GeV LSTs observe in the lower range of energies with low intensity showers that need a large photon collection area. The MST is

able to measure energies from around 100 GeV to a few TeV. Last but not least, the SST will be used to measure the highest energy range up to around 300 TeV, where high intensity showers need a small collection area but many telescopes as their flux is low.

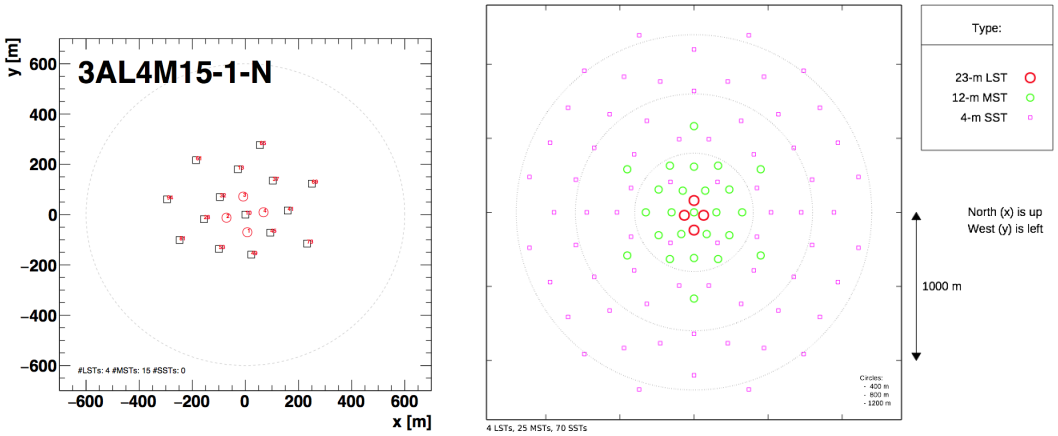

(a) La Palma layout with LSTs (red circles) and MSTs (black squares).

(b) Paranal layout with LSTs (red circles), MSTs (green circles) and SSTs (pink squares).

Figure 7: Proposed array layouts for the North and the South [14].

There are several layout designs for the different telescope sizes proposed.
A layout for the LST with a dish diameter of 23 m is shown in Figure 8. It is also worth mentioning that this year, the first LST will be built on the Canary island of La Palma, the location of the northern array [19].

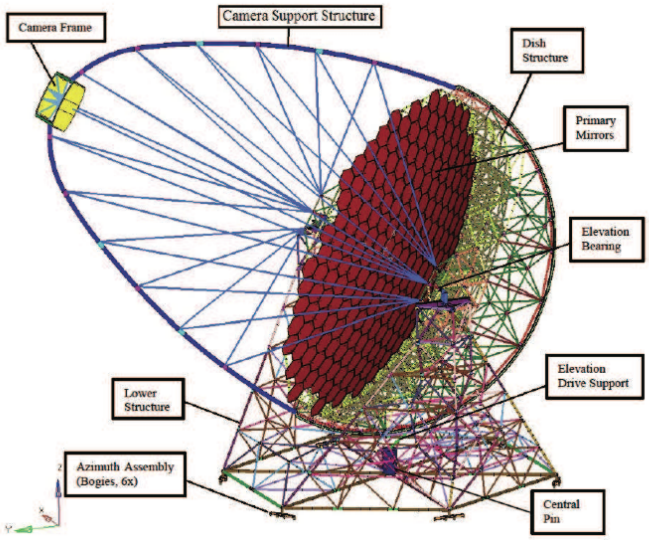

Figure 8: Proposed LST layout for CTA (not final) [19].

For the MST, there are two telescope designs planned: A modified Davies-

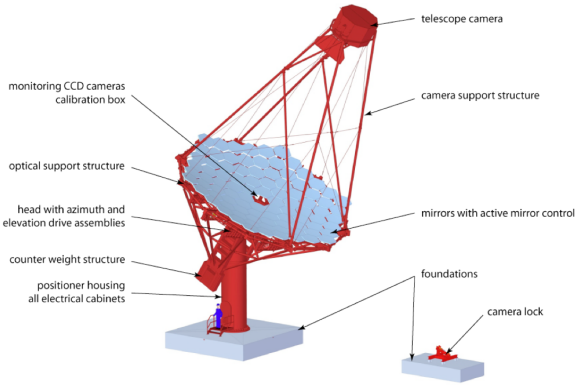

(a) Proposed Davies-Cotton telescope layout for the CTA [11].

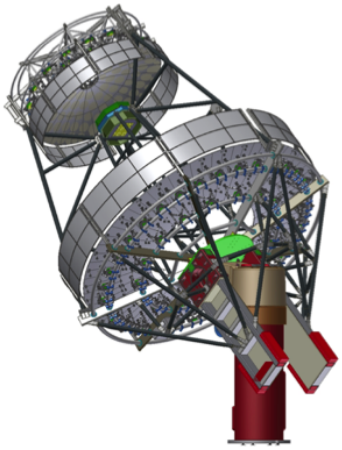

(b) Proposed Schwarzschild-Couder telescope layout for the CTA [15].

Figure 9: Proposed MST designs for CTA

Cotton layout (DC-MST, see Figure 9a) assembled in Berlin in 2012 [11] and a Schwarzschild-Couder design (SCT, see Figure 9b) constructed in Southern Arizona in 2015 [9]. The DC-MST has a dish diameter of 12 m [11] and the SCT a dish with 9.6 m in diameter with an additional secondary mirror of 5.4 m [12]. Among the subarray of SSTs are three proposed telescope designs (see Figure 10), the SST-1M (Davies-Cotton design with one 4 m diameter mirror), the GCT (Gamma-ray Cherenkov Telescope) and the ASTRI (Astrophysics con Specchi a Tecnologia Replicante Italiana) telescope. Both, the GCT and ASTRI, are based on a dual mirror Schwarzschild-Couder design with a diameter of the primary mirror of ~ 4 m and a secondary mirror of 2 m [26], [1].

2.2 Cameras

In this section, only the proposed camera designs for the SCT (proposed telescope design for MST) and the GCT (proposed telescope design for SST) will be described since these are the ones in which the characterized application specific integrated circuit (ASIC) T5TEA will be implemented [29].
The camera proposed for the GCT is the Compact High Energy Camera, in short CHEC, which is able to record fast Cherenkov flashes of a few nanoseconds. A prototype camera with multianode photomultipliers (MAPMs), called CHEC-M, has already been built and tested during 2015.

(a) Proposed SST-1M telescope layout for the CTA.

(b) Proposed ASTRI telescope layout for the CTA.

(c) Proposed GCT telescope layout for the CTA.

Figure 10: Three different design concepts proposed for the subarrays of SSTs for CTA [26].

CHEC-M (see Figure 11) is 0.4 m in diameter and contains 32 camera modules (see Figure 12), each with 64 pixels with a size of $6 \times 6\,\mathrm{mm}^2$, so 2048 pixels are assembled in the whole camera. The camera can be calibrated via LED flashers mounted in the corners and is cooled by liquid.

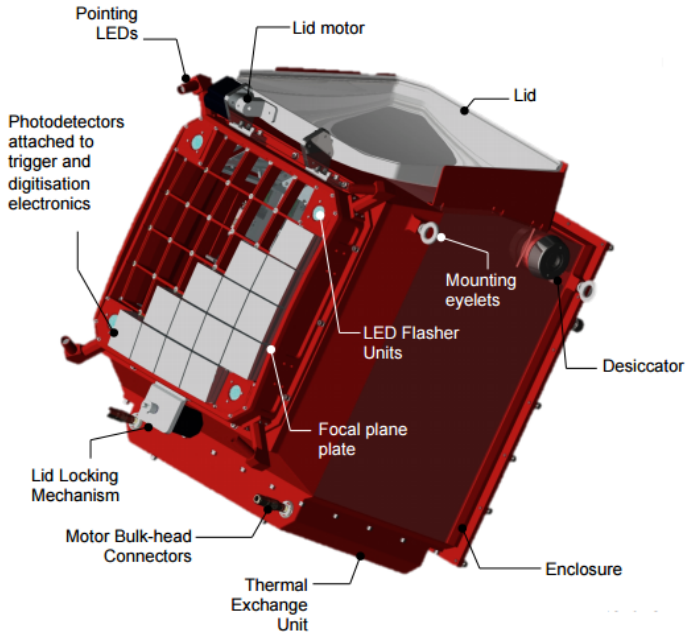

Figure 11: Layout of the CHEC-M camera [1].

One camera module consists of an MAPM, four preamplification boards and one TARGET module (see section 3). The preamplification boards shape the signal properly for the trigger. Simulations show that the optimal shape is $5.5 - 10.5$ ns full width at half maximun (FWHM) and $3.5 - 6.0$ ns rise time. TARGET modules contain four custom designed ASICs, each having 16 input channels for the shaped signal coming from the preamplifier board.

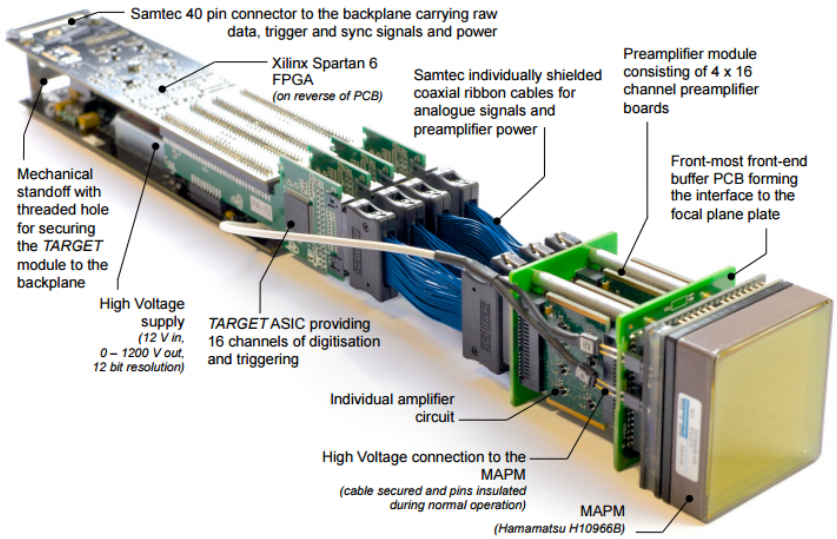

Figure 12: One camera module [1].

All 32 TARGET modules are connected via a backplane board which transfers the data to two DACQ (data acquisition) boards. They transport the signal to the outside world of the camera. The backplane also receives the trigger signal from the TARGET module ASICs and initiates the read out.
A second prototype of a GCT camera, called CHEC-S, is going to have silicon photomultipliers (SiPM) instead of MAPMs [1] and use the newest generation of the TARGET family, T5TEA and TC, as ASICs [29].

The SCT has a different layout for its camera with a size of about half a square meter. It consists of 9 sub-fields with 177 TARGET modules in whole, which have 64 pixels each. In total there are $11,328$ pixels for the whole camera with one pixel corresponding to one SiPM of a size of $3 \times 3\,\mathrm{mm}$. Furthermore, one trigger pixel ($12 \times 12\,\mathrm{mm}^2$) is built out of four read out pixels (2×2 SiPM pixel, see Figure 13).
Behind the SiPMs there is again an amplifing stage to shape the signal to $\sim 10\,\mathrm{ns}$ FWHM. Again, the TARGET modules are assembled together via a similar backplane, which transfers the signal to other trigger levels [6].
The next chapter first describes how the ASICs of the TARGET module work and then how the trigger ASIC T5TEA was characterized.

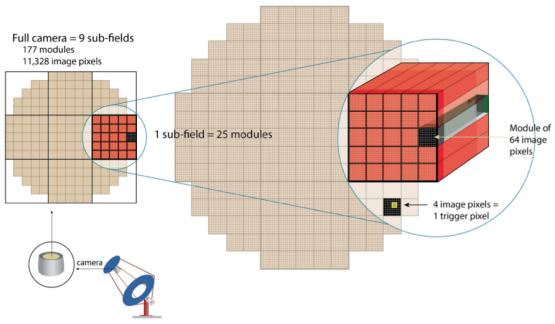

(a) Focal plane of the camera for a SCT.

(b) One camera mechanical support unit for a SCT.

Figure 13: Layout for the camera for the medium-sized Schwarzschild-Couder telescope [6].

3 TARGET

3.1 TARGET ASICs

TARGET is an ASIC designed for sampling and digitizing signals coming from the photosensors of the camera. It is able to trigger on Cherenkov flashes of a few ns and on a few photons, to sample with a high rate ($1\frac{\text{GSa(mple)}}{\text{s}}$) and digitize with 12-bit. The compact design of the ASIC keeps the cost per channel low ($< \$20$), which is advantageous for minimizing the costs for the whole camera [5].
In this thesis an ASIC of the newest generation of the TARGET family, T5TEA, will be presented, where T5TEA stands for TARGET 5 trigger extension ASIC with TARGET 5 being one of the former ASICs [29].
This newest generation of TARGET has a decoupled trigger (T5TEA) and data path (Target C, TC) in order to reduce switching and noise in the trigger path. In addition it reduces digitization time, has tuneable delay steps and has a better control of the noise [20].
The shaped signal ($\sim 10\,\text{ns}$ FWHM) coming from the amplifing board, located in front of the TARGET and behind the photosensors (see subsection 2.2), is fed into T5TEA. T5TEA has 16 channels, which are grouped into four so-called trigger groups as an analog sum, respectively. Additionally, the signal will be inverted, which is important to understand why raising the `TRG_THRES` parameter will lower the threshold, and amplified again to be able to set a precise threshold (see Figure 14).

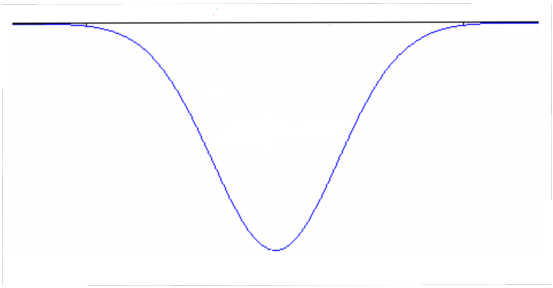

Figure 14: Shaped inverted signal (modified by the author) [16].

A following comparator compares an internally generated `TRG_THRES` parameter to a trigger group which has to be crossed to trigger at a certain value. T5TEA can transfer the trigger signal to a FPGA (field programmable gate array), which can send a read out signal to the sampling ASIC TC, then.
TC samples with a 64-cell switched-capacitor array (SCA[3]), called sampling array, and stores the samples in a $16,384$ cell SCA, called storage array. In contrast to the sampling array, the capacitors are given a new voltage only when the array will be read out or rewritten with new data.
First, one group of 32 cells of the sampling array is sampled while the other group is buffered in the array of the $16,384$ capacitors. In the next half of the sampling

[3]The capacitors in this array work with switches that are opened and closed sequentially to sample the signal [5].

cycle the before mentioned process, with sampling and buffering only one half of the 64 cells, is reversed. Thus, a large bandwidth and a long trigger latency of $\sim 16\,\mu$s is available. This so-called "ping-pong fashion" provides continuous sampling at a rate of around $1\frac{\text{GSa}}{\text{s}}$.
On demand of a controlling device (i.e. an FPGA), blocks of 32 cells from the storage array are going to be digitized with the help of 512 Wilkinson analog-to-digital converters (ADC). All channels are equipped with the same voltage ramp whose rise time can be varied. The ramp is generated by charging a capacitor. Additionally, a 12-bit counter starts independently with a controllable start time. When the voltage ramp crosses the stored voltage the current counter value, which corresponds to the voltage stored in the capacitor of the storage array, is transfered to a shift out register [20]. A scheme of the whole setup can be found in Figure 15.

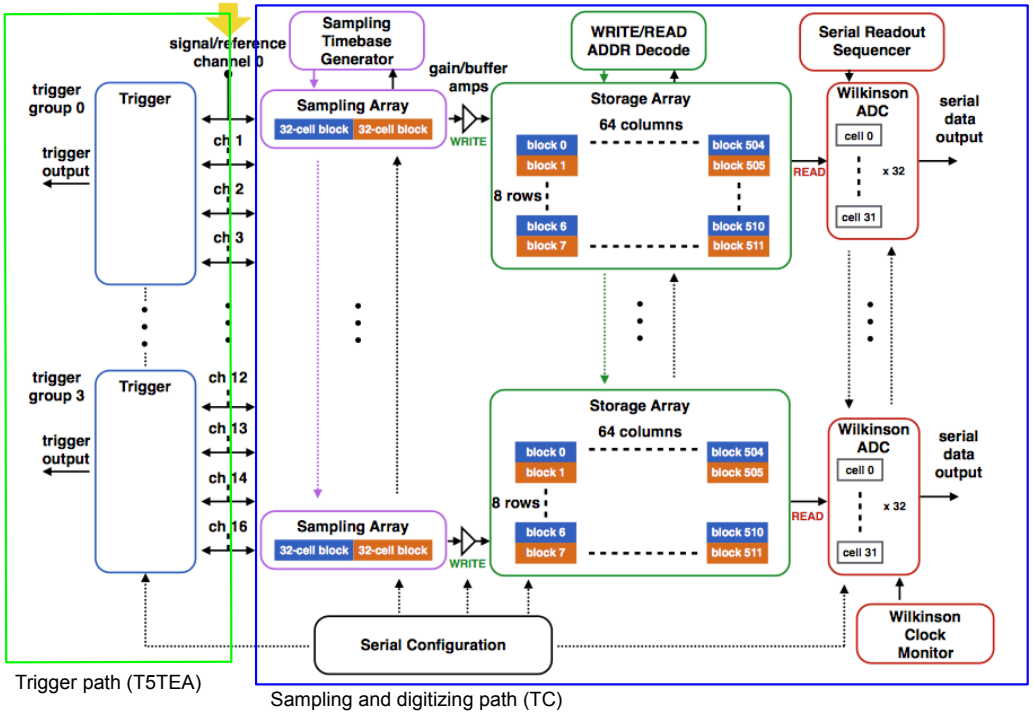

Figure 15: Layout of the TARGET ASICs T5TEA (trigger) and TC (sampling and reading) together (modified by the author) [20].

It has to be mentioned that in the final camera the read out will be initialized at the camera level, not the module level.

3.2 Characterization of T5TEA

In this part, the characterization of the trigger ASIC T5TEA will be presented. This was performed with the help of an evaluation board on which T5TEA, TC and a FPGA, which is controlling the ASICs (see Figure 16), are located.

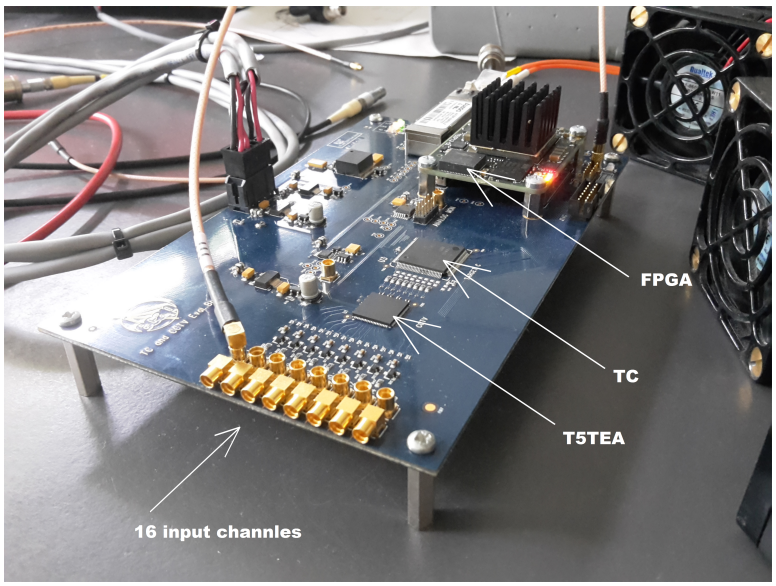

Figure 16: Evaluation board with the 16 input channels, T5TEA, TC and the FPGA.

To get an idea of the trigger, one can find a trigger rate versus threshold plot in Figure 17. On the left one can recognize a raise from zero to ten trigger counts, with ten corresponding to one hundred percent trigger efficiency (see subsubsection 3.2.2). On the right a sudden raise in the trigger rate up to $1.3 \cdot 10^5$ is recognizable which reflects the case when the threshold is set within the baseline of the signal and therefore, the T5TEA triggers at the baseline. Fitting a Gaussian gives the width of the noise.

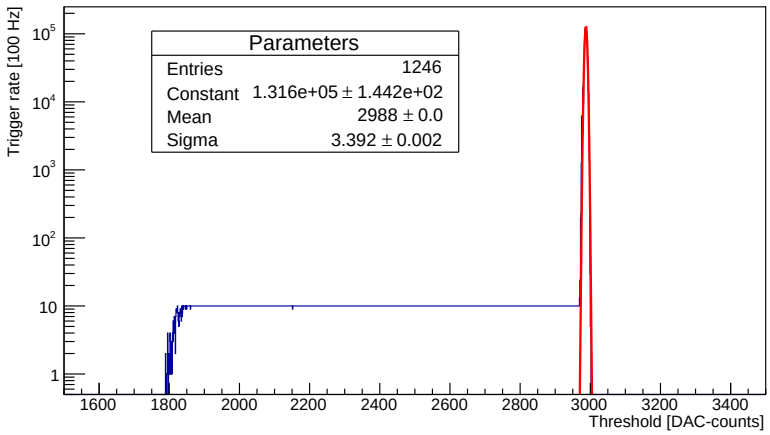

Figure 17: Trigger rate versus set comparator threshold. The parameter "Sigma" denotes the width of the baseline and "Constant" the maximum trigger rate.

Here, only the plot for channel 1 (trigger group 1) of all the 16 channels is shown. Three more plots can be found in subsection A.1.
It can be seen that if the `TRG_THRES` value is set higher, is gets closer to the signal and so trigger signals (see Figure 18) will be sent out.

The applied signal was generated by a function generator with a FWHM of 10 ns, an edge time of 5.4 ns and an amplitude of 100 mV. This shape is approximately as the shape of a signal coming from the SiPMs after shaping, except for the amplitude. Here, the amplitude was set this high only to illustrate with Figure 17 how the trigger works.

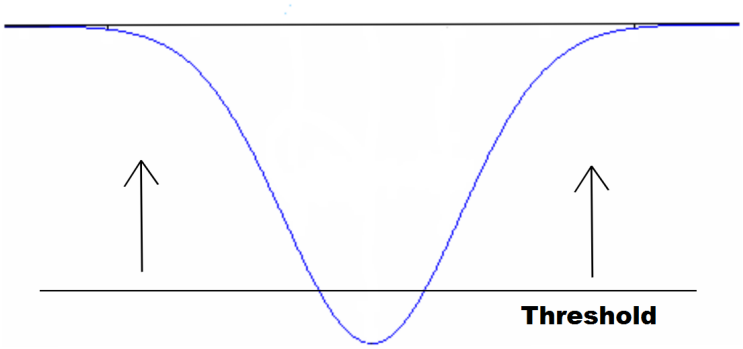

Figure 18: Illustration of getting trigger signals with varying the `TRG_THRES` value (modified by the author) [16].

There are several parameters that have influence on the trigger:

- `VPED` is a parameter that can be set for all channels separately. It is a pedestal (offset) voltage that shifts the signal into the dynamic range[4] of the transfer function of TC and into the working range of T5TEA. It can be generated internally in the case of T5TEA.
- `TRG_THRES` sets the comparator threshold that has to be crossed to trigger and can be set for each trigger group.
- `PMTREF4` shifts the summed signal closer to the comparator threshold to trigger small pulses and it also can be set for each trigger group.
- `WBIAS` changes the width of the trigger output pulse, trigger groupwise.

All the parameters are given in counts from 0 to 4095 provided by a 12-bit DAC and correspond to a voltage range of 0 to 2.5 V.
The following measurements were performed with a frequency of 1 kHz and an load impedance of 50 Ω, which will be set on the function generator, unless something else is mentioned.

3.2.1 Transfer function

External measurement The transfer function connects the set `VPED` in DAC counts to the analog voltage. Here, `VPED` values were provided to T5TEA and the voltage was measured externally by a voltmeter. This was carried out for all

[4]The dynamic range is the range of the transfer function that behaves monotonic increasing (see subsubsection 3.2.1).

channels in order to investigate whether they all behave the same way and for calibrating the TC ASIC later on. An example of a transfer function is given in Figure 19 for channel 14 (trigger group 4), with a dynamic range of about 2 V. This means that there is a large range to work in where it is easy to set DAC counts and convert them into mV.
Indeed, all the channels behave similar (see subsubsection A.2.1).

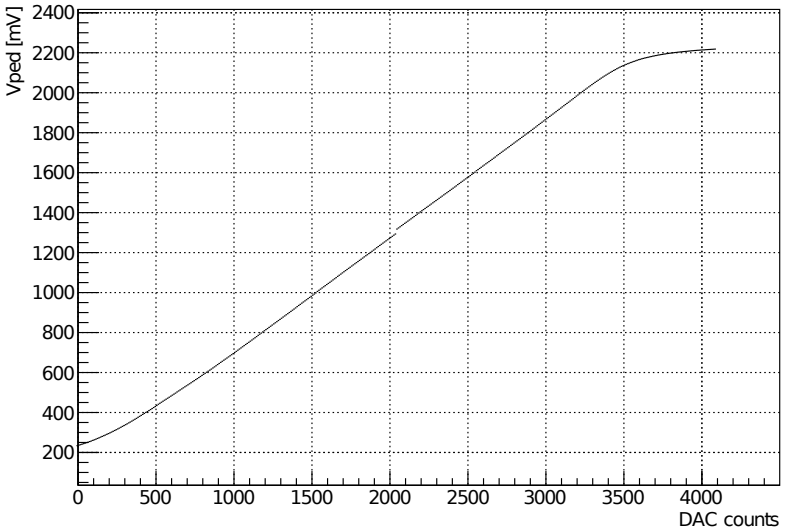

Figure 19: Transfer function for channel 14 (trigger group 4) with a jump at 2048 DAC-counts.

The jump at 2048 DAC-counts is investigated in detail in Figure 20. In this figure, the step height from one DAC-count to another (in steps of one) in mV is plotted against the corresponding count, but only in the range where the transfer function is monotonic increasing. Looking closer, one can observe that there is one big step with a value of about 20 mV and several little jumps with various values that occur more or less regularly in intervals of around 100 counts. This can be tied to the fact that the converter is working with a voltage divider of twelve different resistors (bits), which are "connected" via switches. When a bit (or rather a resistor) gets connected to another one, the voltage from one count to the next is going to be different with respect to the tolerances of the resistors involving.

Internal measurement - TC transfer function In this measurement, the `VPED` values were set in DAC-counts, converted into voltages as it was shown in the previous measurement (see External measurement) and measured in ADC-counts by TC. Here, one block of 32 cells of the storage array was digitized.

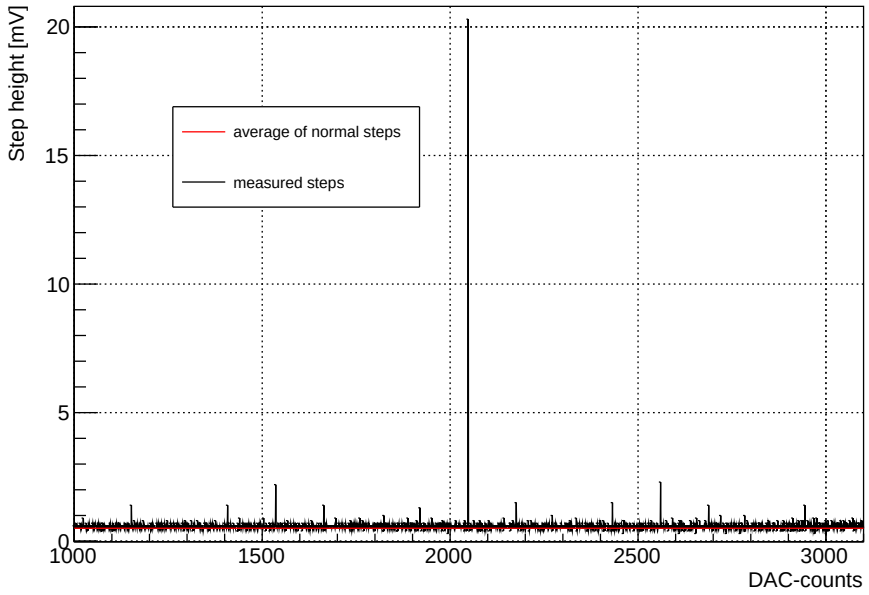

Figure 20: Step heights of the voltage applied for each DAC-count for channel 14.

In order to get some statistics and reduce errors there were more events taken for each cell and `VPED` value. Therefore, a histogram was filled and one can read out the mean (see Figure 21) and RMS value (TC and T5TEA noise, see Figure 22). Figure 21 and Figure 22 illustrate the measurement performed for channel 2. The different colors represent the different cells. It is worth mentioning that the read out mechanism for channel 1 did not work properly, so the first channel that was measured is channel 2.
One can observe that all cells act the same way except for cell 32 (pink line), which lies beneath. This behavior can also be observed for the TARGET generations before and can be calibrated. To explain that there need to be carried out further measurements.
The monotonic increasing of the curve starts around 0.6 V, which results in a dynamic range of about 1.6 V. The maximum voltage of TC of 2.5 V can not be reached with the `VPED` of T5TEA because the `VPED` is only extended up to 2.2 V (see Figure 19). Additional measurements with an external `VPED` were performed, showing a dynamic range of 1.9 V and an integrated non-linearity[5] of ≤ 70 mV (see Figure 23, [27]).
The cell with the yellow line behaves differently than the other ones, which have the same height of noise, and has to be investigated further. Also more plots for channel 6 and 14 can be found in the appendix (see subsubsection A.2.2).
Just like for channel 2, cell 32 again acts differently than the other ones for channel 6 and 14. This leads to the assumption that something is wrong with this cell and it doesn't depend on the channel.

[5]The integrated non-linearity is the deviation of the ideal ADC-counts with respect to the actual measured counts [29].

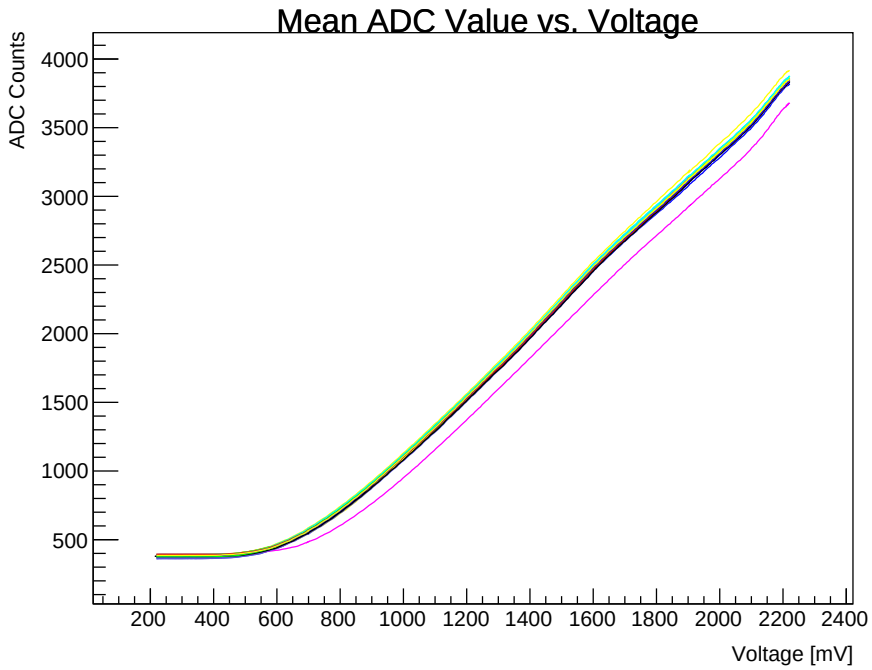

Figure 21: Mean of measured ADC count versus `VPED` measurement for channel 2.

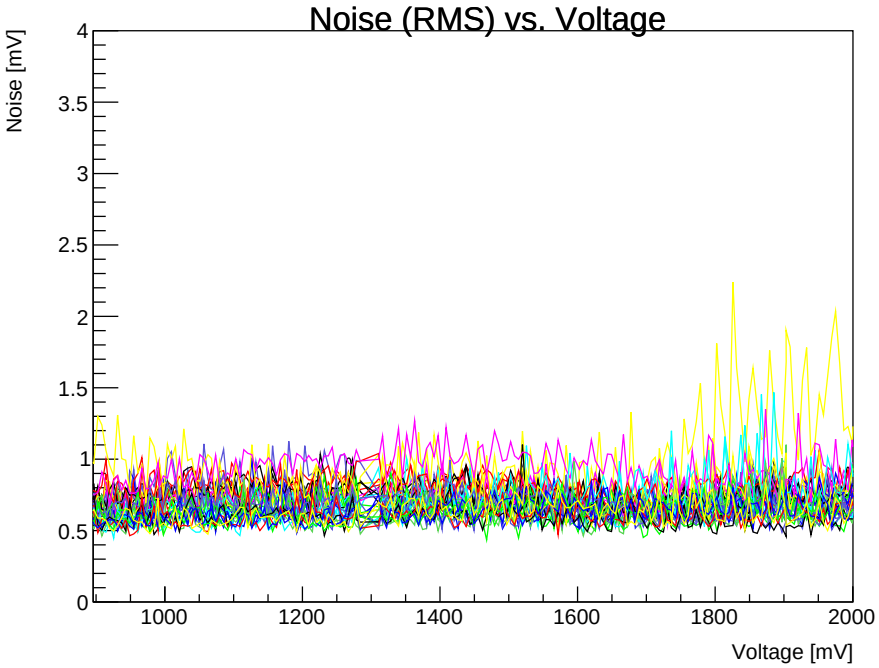

Figure 22: RMS of measured ADC count versus `VPED` measurement for channel 2.

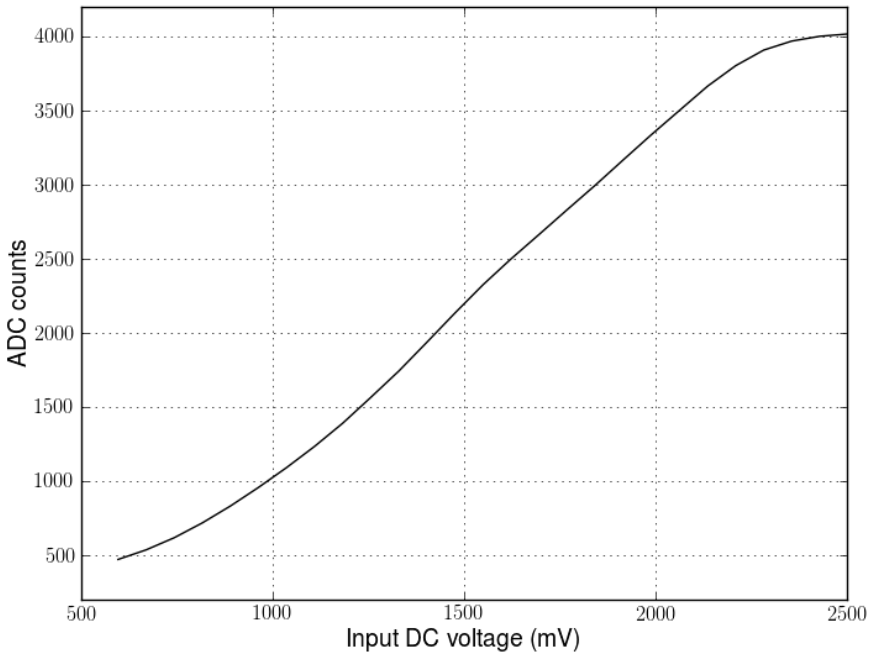

Figure 23: Measurement with external applied `VPED` [27].

Taking a look at the noise plots in the appendix, one observes that channel 6 has a much larger noise of $\sim 1.5\,\mathrm{mV}$ than the other channels. On the other hand, channel 14 has a very low noise of $0.5\,\mathrm{mV}$. To give an explanation, this has to be investigated further.
The transfer function of TC can be compared to the T5 transfer function, which can be found in Figure 24. Here, `VPED` was not applied internally but externally. By comparing the dynamic ranges (T5TEA: 1.6 V (internally), 1.9 V (externally); T5: 1.2 V) one can recognize that the one of T5TEA is a little bit better, which is very promising.

3.2.2 Trigger efficiency

The trigger efficiency was measured in a way that the function generator sets different input pulse amplitudes ($\sim 1 - 12\,\mathrm{mV_{pp}}$, $0.2\,\mathrm{mV}$ steps). At a certain value, T5TEA is able to trigger, while the trigger efficiency is $\frac{\text{number of trigger}}{\text{number of pulses}}$, which depends on the amplitude. The division by the number of pulses was done because the frequency and the read out time was set in a way that we expect a certain number of trigger signals. So by dividing the number of triggers by the number of pulses we get the trigger efficiency in percent. Figure 25 shows one example how the trigger efficiency curve looks like. A Gaussian error function was fitted to the measured points in the following form:

$$f(x) = \frac{1}{2}\left(1 + \mathrm{erf}\left(\frac{x-\mu}{\sqrt{2}\sigma}\right)\right), \tag{1}$$

with μ being the mean value with 50% efficiency (threshold) and σ the spread around the mean value (noise). Both are given in mV.

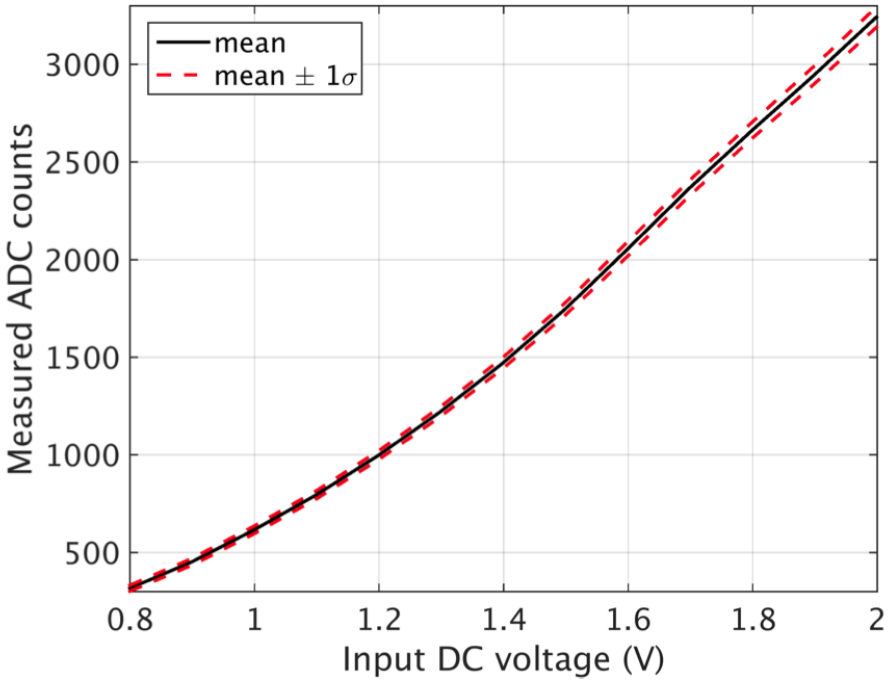

Figure 24: Dynamic range of the transfer function of the previous ASIC T5 [5].

Channel 1 is able to trigger at a mean value of $\mu = (7.029 \pm 0.025)\,\mathrm{mV}$ and has a noise of $\sigma = (0.777 \pm 0.038)\,\mathrm{mV}$. The requirement for the whole camera that should be met is to trigger at 80 p.e.[6] per a definite area with 50% efficiency, which means $\sim 10\,\mathrm{mV}$ as a requirement for the mean value for each channel. All the channels meet the requirement of about 10 mV for the mean value.
For the plot shown in Figure 25, the trigger dependent parameters were as follows:

- `VPED` = 1000
- `TRG_THRES` = 2930
- `PMTREF4` = 1980
- `WBIAS` = 985.

Trigger efficiencies of other channels and their parameters for the trigger can be found in subsubsection A.3.1.

[6]The abbreviation p.e. stands for photoelectron. Photoelectrons will be created by the phenomenon of the photoelectric effect, where electrons leave the surface due to incoming optical photons with energies of approximately $1 - 3\,\mathrm{eV}$.

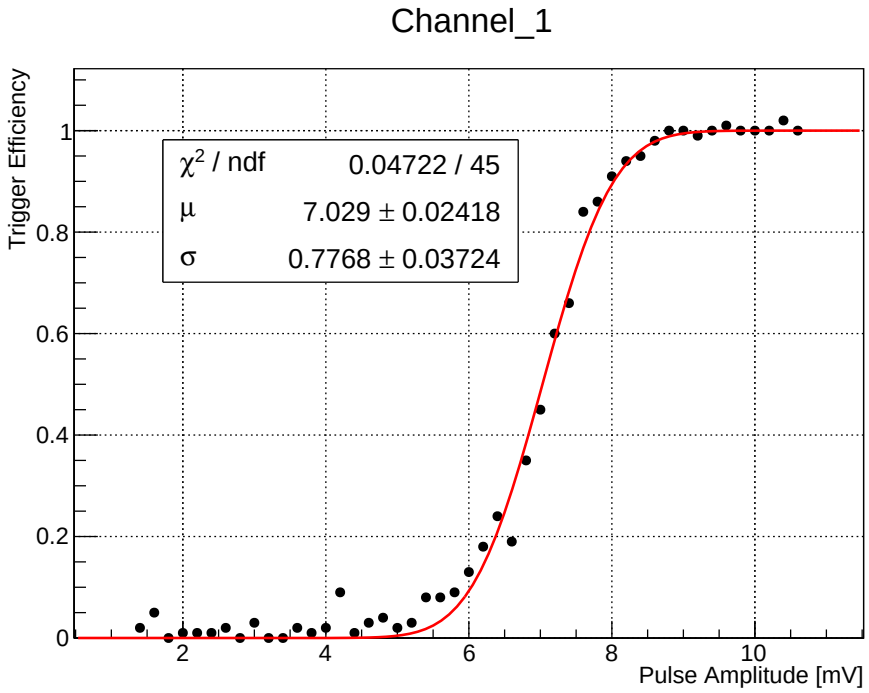

Figure 25: Trigger efficiency of channel 1 (trigger group 1) with the fit function (red line).

For most efficiencies the mean values are almost the same within one trigger group. But channel 16 works better than the other channels in its trigger group. More measurements should be performed to investigate this in more detail, to explain the difference and perhaps find better parameters for the trigger.
To get approximately the same mean value for all channels the pedestals of all channels in one group have to be the same. Therefore, the `VPED` value for the first channel of one trigger group was set to 1000 and then a value for `TRG_THRES` with a low threshold was searched. The corresponding voltage to the 1000 DAC-counts of the first channel was looked up in the transfer functions of other channels and with that, the proper DAC-counts to the voltage were found. With this scheme the `VPED` for each channel is set in a way that approximately the same threshold values within one trigger group (same `TRG_THRES`) were found.
It also has to be mentioned that the values shown here, as well as shown in the appendix, are not the best ones, with better tuning, thresholds of about 4 mV can be reached. The plots in this thesis should only demonstrate that the channels within one trigger group behave similarly. `PMTREF4` was set in a way that the signal is already close to the comparator threshold.
All measurements were done with an load impedance, set on the function generator, of 50 Ω as explained before, which give results that are overestimated. As a consequence the applied pulse is bigger than what is shown by the function generator. There was made a trigger efficiency measurement with the correct impedance of 410 Ω (set at function generator) for channel 1 (see Figure 26).

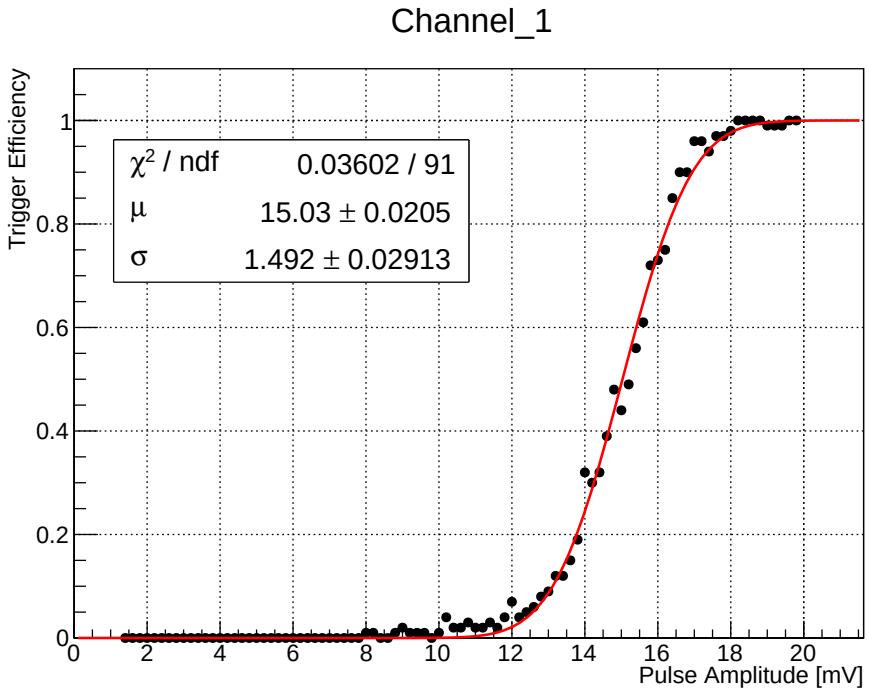

Figure 26: Trigger efficiency with a load impedance of 410 Ω (set on function generator) for channel 1.

One can observe that the results are worse with respect to Figure 25, with a mean value of 15 mV and a noise of 1.5 mV. The other trigger efficiencies can be found in the appendix (see subsubsection A.3.2).
Important to mention is that the sampling of TC was enabled. Figure 27 shows the trigger efficiency of T5 (sampling enabled), which is worse ($\mu = 35\,\text{mV}$, $\sigma = 5.4\,\text{mV}$) compared to T5TEA ($\mu = 15\,\text{mV}$, $\sigma = 1.5\,\text{mV}$).

3.2.3 Pulse widths

Input pulse - Threshold versus width measurement To investigate how T5TEA handles different input pulse widths, measurements with varying pulse widths were carried out. The pulses were broadened in steps of 1 ns and at each value, efficiency curves were measured. This has been done for all channels, e.g. Figure 28 shows the measurement for trigger group 1.
The trigger parameters were the same as in the former measurement (see subsubsection 3.2.2). As expected, the threshold gets lower with increasing width of the signal.
This can be explained by the fact that the comparator output produces a pulse with a width corresponding to the time over threshold, which is used as a clock for the output pulse. The signal has to be above the threshold for a certain amount of time to be able to control the electronics. When the signal has a large width, the goal of hitting the defined length is easier. As a consequence of that, the trigger threshold with 50 % efficiency is reached at higher input pulses at smaller widths.

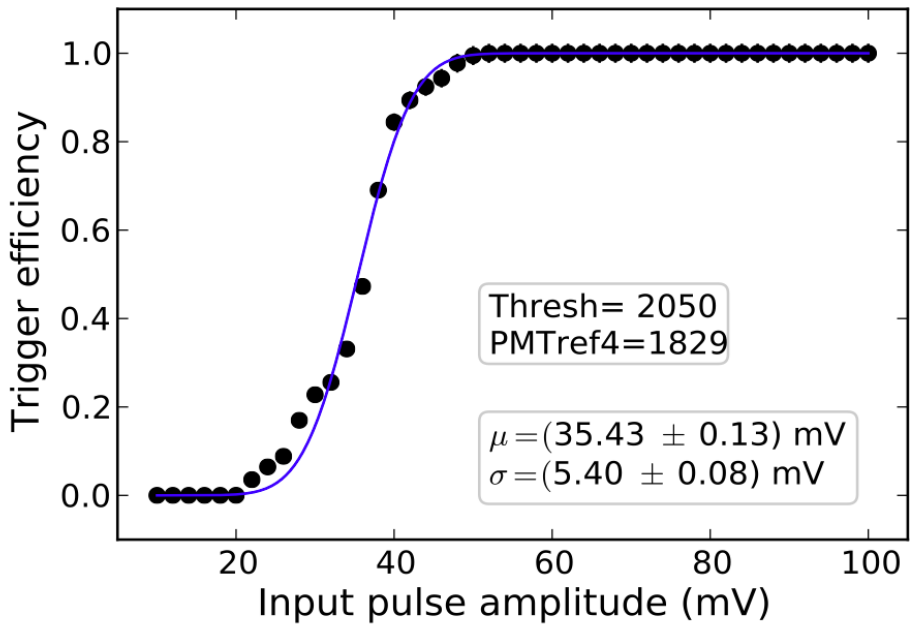

Figure 27: Trigger efficiency of T5 [5].

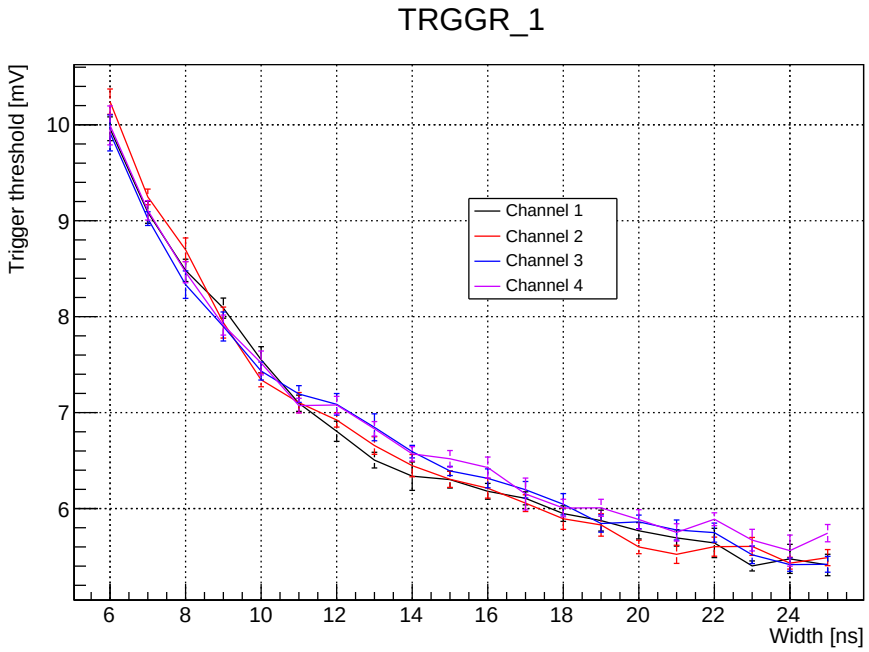

Figure 28: Threshold with 50 % efficiency versus width measurement for trigger group 1.

Plots for the other trigger groups are shown in subsection A.4.
Unlike trigger groups $1-3$, trigger group 4 behaves not in the same way. In general, trigger group 4 is worse with respect to the others with the exception of channel 16. This channel again behaves differently than the others in its trigger group and has to be investigated further to find the reason for that.

Output pulse - Width versus `WBIAS` measurement As mentioned at the beginning of this chapter, `WBIAS` varies the width of the output pulse of the trigger. Here, `WBIAS` was set in DAC-counts and the width was measured in ns with an oscilloscope.
Additionally, the measurement was performed before and after the FPGA in order to investigate how the FPGA influences the signal.
Figure 29 shows the measurement for channel 1 with an input pulse of 15 $\mathrm{mV_{pp}}$.

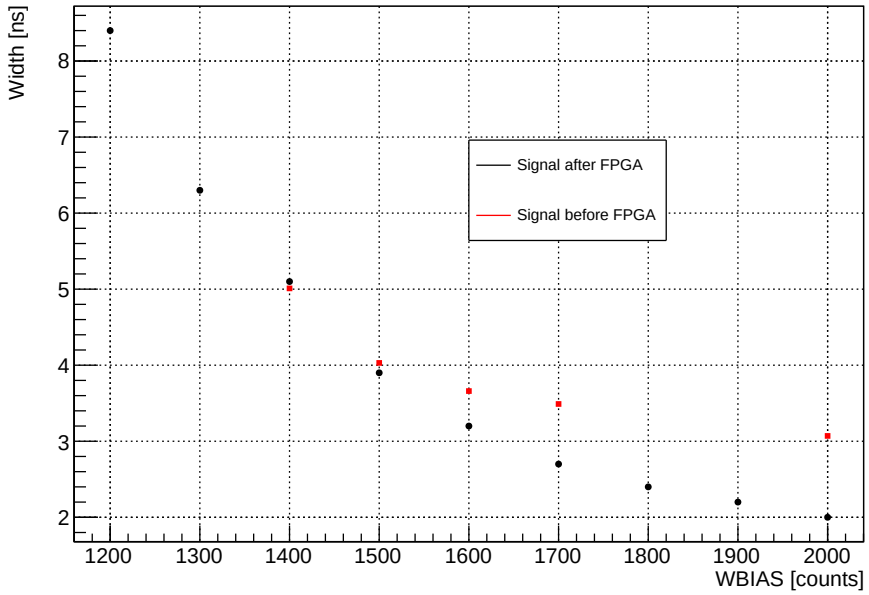

Figure 29: Width versus `WBIAS` plot for channel 1. The signal measured before the FPGA is tagged with red dots and after the FPGA with black dots.

The behavior can be described in the way that with increasing `WBIAS` the width of the output signal gets smaller. An explanation is that with increasing `WBIAS` the trigger output signal will be pulled faster to zero. A more detailed explanation would be too technical and would break the framework of this thesis.
For a `WBIAS` of 2000, the width of the output pulse of T5TEA was measured to be 2.0 ns (signal after FPGA), which meets the requirement of about 4 ns.
The number of measured datapoints for the signal before the FPGA is less than for the signal after the FPGA because the values were probed, other then the signals behind the FPGA, using distinct coax connectors to get only an idea of the relation between the width and `WBIAS` before the FPGA.
Moreover, one recognizes that there is a difference between the signal before and after the FPGA of 1 ns around 2000 counts. The FPGA shapes the signal before it gets passed, which causes the just mentioned difference in the width.
The datapoints measured for the signal after the FPGA can be compared to T5 (see Figure 30).

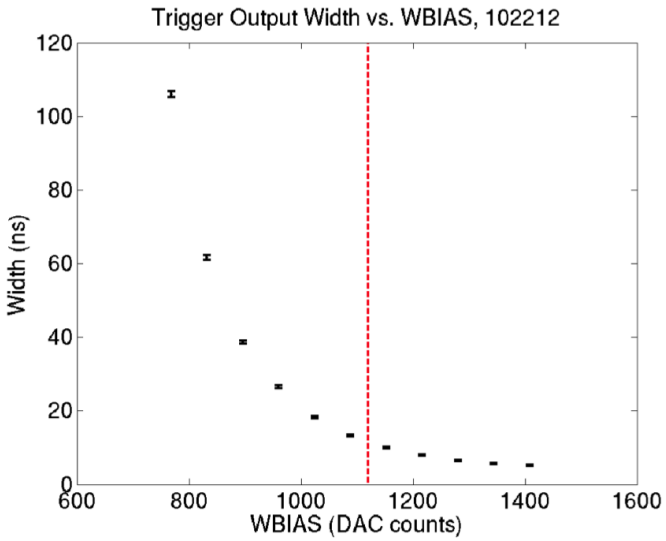

Figure 30: Width versus `WBIAS` measurement for T5 [23].

It can be assumed that T5 and T5TEA behave the same way in the lower range of the width.

3.2.4 `PMTREF4` versus `TRG_THRES` measurement

To derive good parameters for `PMTREF4` and `TRG_THRES` a scan through the `PMTREF4`-`TRG_THRES` plane was performed. This was realized by setting `PMTREF4`, ranging from $0-4095$ counts and measured in steps of 5 counts, and going through the `TRG_THRES` values, also ranging from $0-4095$ counts (set in steps of 10). For each `TRG_THRES` value the function generator sent pulses with amplitudes between 1 mV and 50 mV in steps of 1 mV, a width of 10 ns and an edge time of 5.4 ns. The step length of 1 mV was changed to 0.2 mV as soon a trigger was found.
In order to reduce data, the recording of trigger signals stopped when there were eleven triggers with approximately 100 % efficiency measured. Figure 31 shows a measurement done with channel 1, a `VPED` value of 1000 counts and a `WBIAS` of 985 counts corresponding to a width of the output pulse of about 21.1 ns. The mean value can be seen color-coded on the right side of the plot. The best ranges to carry out measurements can be picked between 1800 and 2000 `PMTREF4` counts and 1200 and 3100 `TRG_THRES` counts with a mean value of about 4 to 5 mV.
The noise was measured as well (see Figure 32). With values ranging from 1900 to 2100 counts for `PMTREF4` and for `TRG_THRES` counts from 2700 to 3400, the noise was relatively low at around 0.5 mV. At the left and right side (white areas) of the measured thresholds and RMS there were also triggers found but not measured for the plot. Trigger signals were only measured when there was a first trigger signal found around 10 mV (left area). The white area on the right is caused because there were more triggers found than expected which is due to `TRG_THRES` values moving into the baseline (see subsection 3.2).

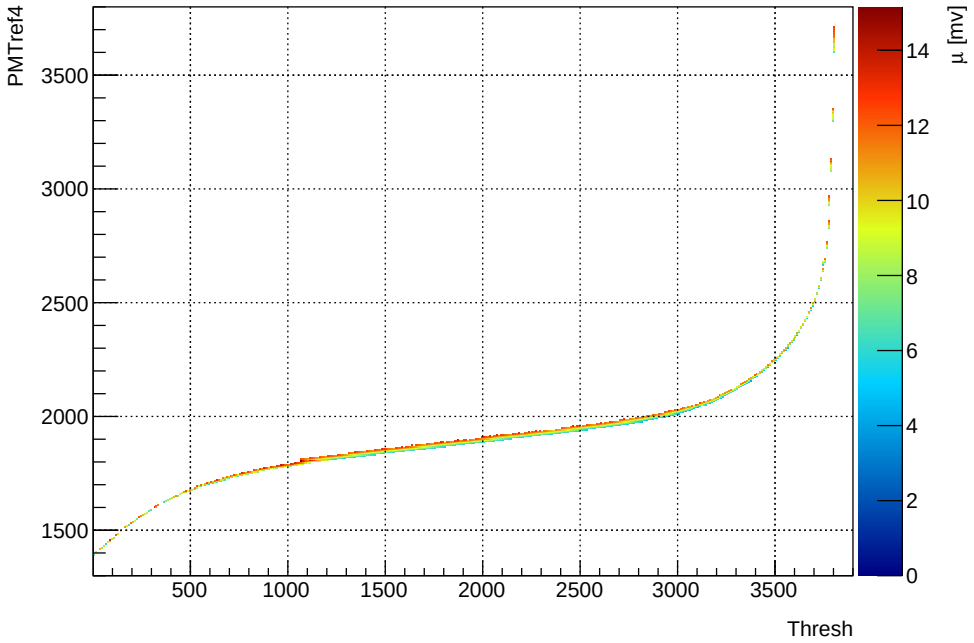

Figure 31: PMTREF4 versus TRG_THRES measurement with a color-coded mean value.

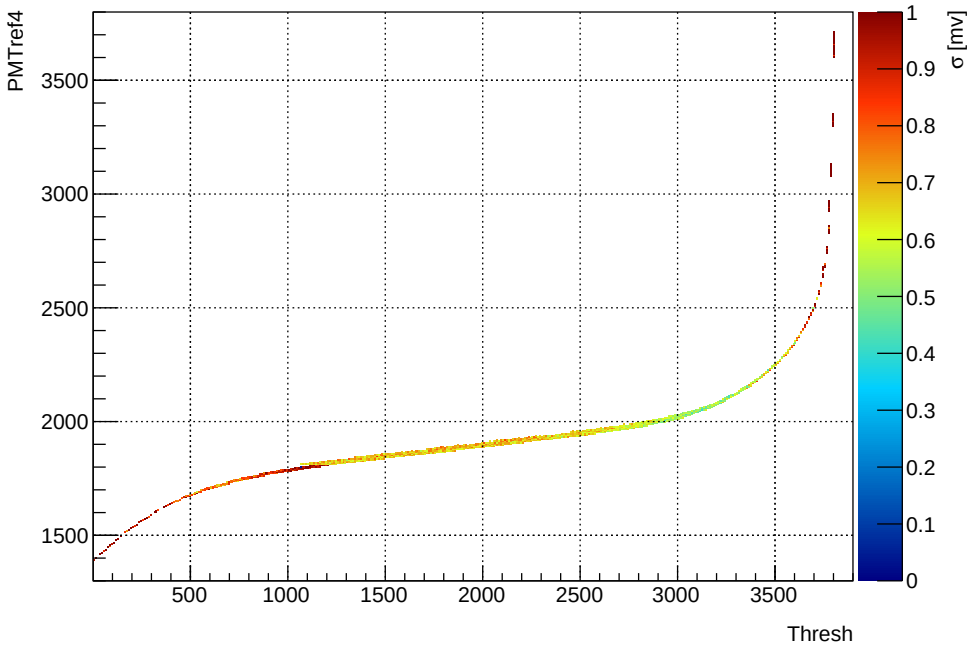

Figure 32: PMTREF4 versus TRG_THRES measurement with a color-coded sigma value.

The same measurements were perfomed for T5 and the results can be found in Figure 33. There, the axes are changed and there is a zoomed view in the TRG_THRES-PMTREF4 plane.

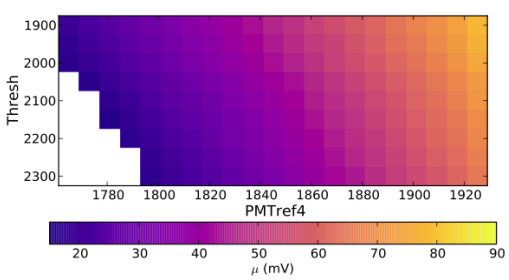

(a) TRG_THRES versus PMTREF4 measurement with color-coded mean value at the bottom.

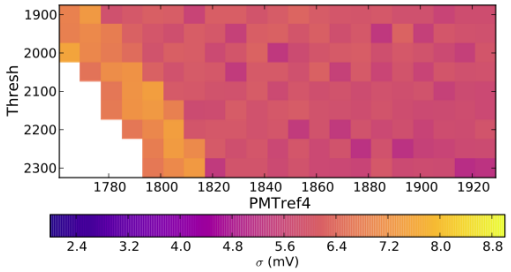

(b) TRG_THRES versus PMTREF4 measurement with color-coded sigma value at the bottom.

Figure 33: TRG_THRES versus PMTREF4 measurement for T5 [5].

To compare the two results, a scan with smaller parameter ranges was carried out (see Figure 34).

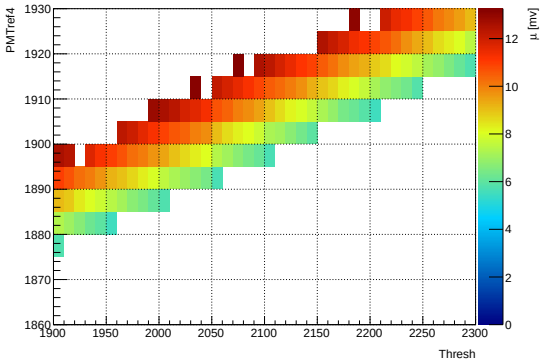

(a) TRG_THRES versus PMTREF4 measurement with color-coded mean value at the right.

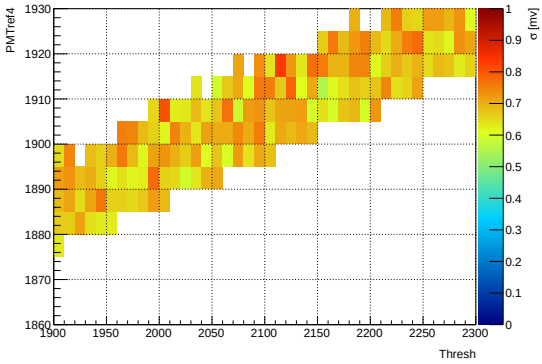

(b) TRG_THRES versus PMTREF4 measurement with color-coded sigma value at the right.

Figure 34: TRG_THRES versus PMTREF4 measurement for T5TEA.

As before, T5TEA triggers at lower thresholds of $\sim 6\,\mathrm{mV}$ than T5 ($\sim 20\,\mathrm{mV}$).

3.2.5 Noise versus threshold measurement

To get an idea of how the channels behave within one trigger group for different TRG_THRES values with respect to the noise and mean value, a measurement to investigate this behavior was carried out. The measurement started around 50 mV, which was the TRG_THRES value at which the first trigger appeared and was set to higher ones in steps of 100 counts. When reaching $\sim 10\,\mathrm{mV}$ the steps were set to 10 counts. The measurements were repeated ten times to get more statistics (see error bars in Figure 35).
For all measurements the parameters shown in the table in subsection A.3 were used except the one for TRG_THRES as this that parameter was varied. A noise-threshold-plot of trigger group 1 can be found in Figure 35.

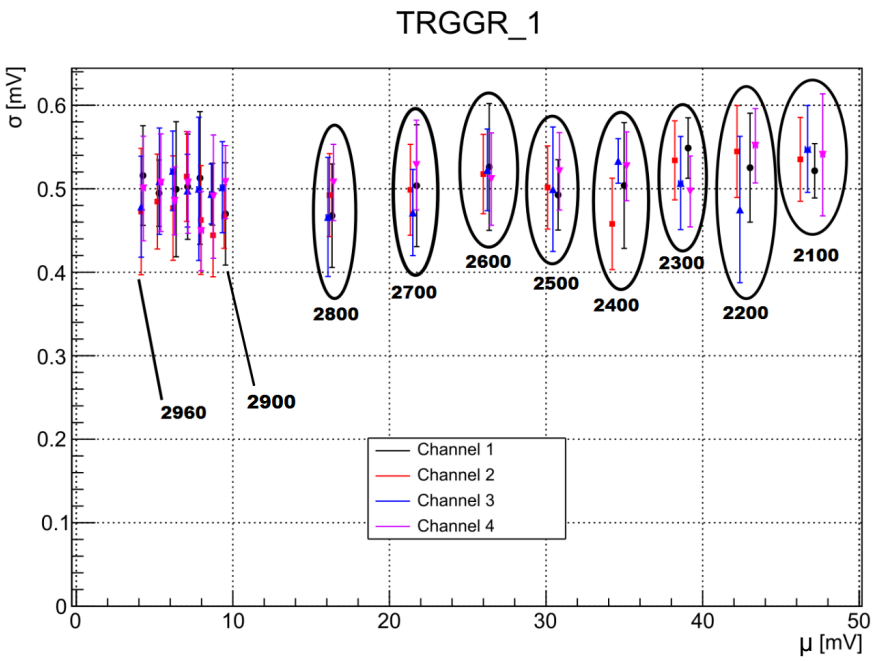

Figure 35: Noise versus threshold measurement for trigger group 1. The black ellipses (or black lines) mark the set `TRG_THRES` value.

It can be observed that the noise (sigma) stays almost the same at around 0.5 mV. In addition, there can be seen that at higher thresholds the measured values for one `TRG_THRES` spread a little bit but at lower thresholds they are the same. This might be because the spread is simply larger at higher thresholds compared to lower ones. The lowest trigger threshold of ~ 4 mV can be recognized at 2960 `TRG_THRES` counts. Plots for the other trigger groups can be found in subsection A.5. Compared to trigger group 1, trigger group 2 behaves slightly different. In general, it shows a higher noise, beginning at 0.9 mV it drops down to 0.7 mV with increasing `TRG_THRES`. 6 mV is the lowest trigger threshold at a `TRG_THRES` count of 3120. Channel 5 behaves like the channels in trigger group 1, which has to be investigated further.
The behavior of trigger group 3 is just similar to trigger group 2 with the exception that the lowest threshold is at 3170 `TRG_THRES` counts.
Last but not least, trigger group 4 is worse because it shows the lowest trigger threshold of ~ 10 mV with 2760 `TRG_THRES` counts. Again, channel 16 is behaving differently in contrast to the others. For this channel the smallest threshold is at 5 mV.

4 Summary and outlook

Summary

Concluding from the results obtained by the measurements presented in this thesis, the trigger ASIC T5TEA meets almost all requirements needed for triggering on very short events of Cherenkov flashes.
The signals, on which T5TEA should be able to trigger with 50 % efficiency, will be in the range of a FWHM of 10 ns and an edge time of 5.4 ns. T5TEA triggers on them with a threshold of 15 mV (410 Ω load impedance), which is in the vicinity of the 10 mV requirement. Former ASICs weren't able to trigger at such low thresholds, e.g. T5 had a minimum threshold of 35 mV.
T5TEA handles input pulses with larger width differently than the narrow ones, with increasing FWHM the threshold of the trigger gets smaller.
`PMTREF4` and `TRG_THRES` are the most important parameters that have an influence on T5TEA and were therefore scanned to get ranges where the trigger threshold is small.
The width of the output signal from T5TEA can be varied with the `WBIAS` parameter down to 2.0 ns. T5 has the same behavior for this measurement.
In almost all measurements the trigger groups behaved the same way but channel 16 was always slightly better compared to the other channels within its trigger group.
The transfer function of the sampling ASIC TC features a dynamic range of about 1.9 V and is therefore slightly better than the 1.2 V of T5. In this thesis, the pedestal values were provided by T5TEA.
All channels show a jumpy transfer function which is due to the voltage divider working as a 12 bit counter consisting of resistors with slightly different tolerances.

Outlook

There are several next steps to characterize T5TEA in more detail.
First to mention is that a tuning of the evaluation board of T5TEA, with a big improvement of the trigger efficiency (see Figure 36) down to 3 mV, was performed. This time the 50 Ω load impedance, which is set on the function generator, is correct and the parameters were the same except `TRG_THRES`. `TRG_THRES` was modified a little bit in order to trigger at lower thresholds without moving into the baseline. For channel 1, `TRG_THRES` was set to 2970 counts. An improvement of about 12 mV can be recognized on contrary to the former measurement with the old evaluation board setting (15 mV trigger threshold, see subsubsection 3.2.2).
Due to the improvement of the trigger threshold, all measurements should be carried out again to look if there are other changes as well.
By scanning through all parameters that have influence on the trigger, better values to improve the thresholds can surely be found, but in course of this thesis there was not enough time to run this scan.
Also, one should take a closer look at channel 16 which behaved always differently within its trigger group.

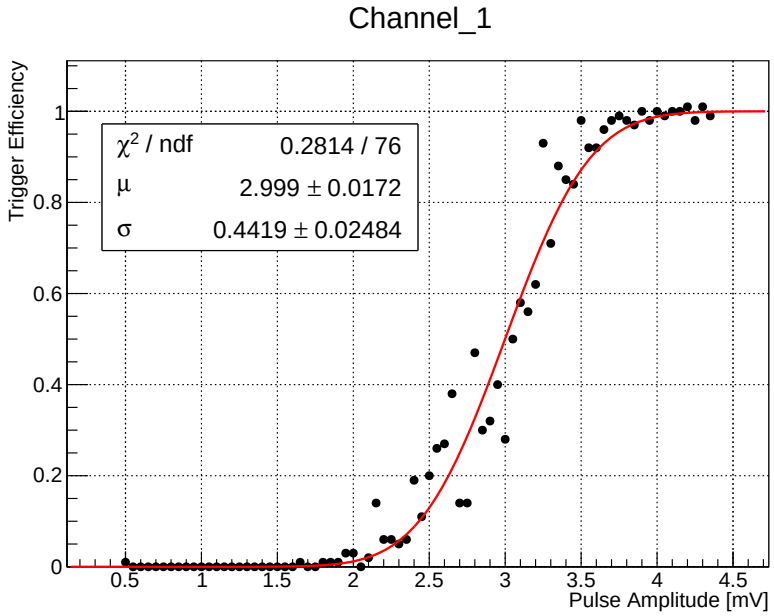

Figure 36: Trigger efficiency for channel 1 with the modified evaluation board.

In addition, in the near future there will be performed measurements with additional components (buffer board and shaper), which are needed to build the whole read out chain.
Similar measurements, as presented in this thesis, should be performed with varying temperature to look whether the ASICs can handle temperature variations, which occur at locations like LaPalma or Paranal.

A Appendix

Besides the investigated parameters there are other parameters that have an influence on the trigger. They were always set to:

- `TTBIAS` = 1100
- `TTBIAS_C` = 1000
- `VPEDBIAS` = 1800
- `TRGSUMBIAS` = 2400
- `TRGGBIAS` = 1900
- `TRGBIAS` = 1000
- `TTBIAS_A` = 400.

A.1 Trigger rate vs threshold measurement

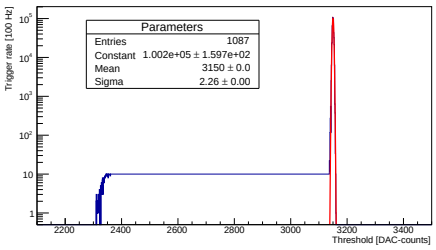

(a) Trigger rate vs threshold plot for channel 5 (trigger group 2).

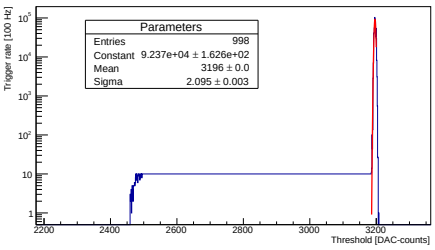

(b) Trigger rate vs threshold plot for channel 9 (trigger group 3).

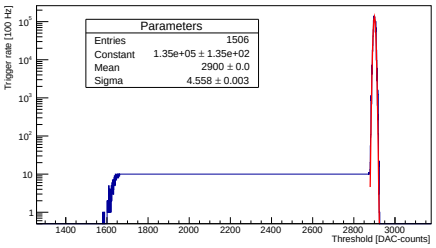

(c) Trigger rate versus threshold plot for channel 13 (trigger group 4).

Figure 37: Trigger rate vs threshold measurements for different channels from different trigger groups.

These are only representatives for each trigger group. The other channels behave the same.

A.2 Transfer function measurement

A.2.1 External measurement

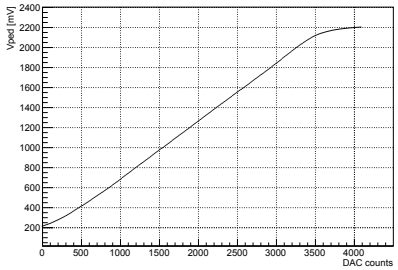

(a) Transfer function for channel 1 (trigger group 1).

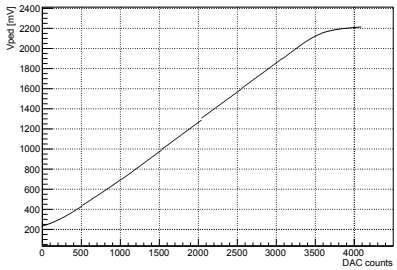

(b) Transfer function for channel 6 (trigger group 2).

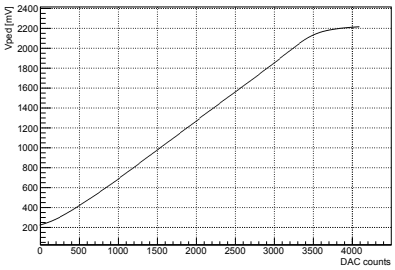

(c) Transfer function for channel 9 (trigger group 3).

Figure 38: Transfer function for different channels of different trigger groups.

These are only representatives for each trigger group. The other channels behave the same.

A.2.2 Internal measurement - TC transfer function

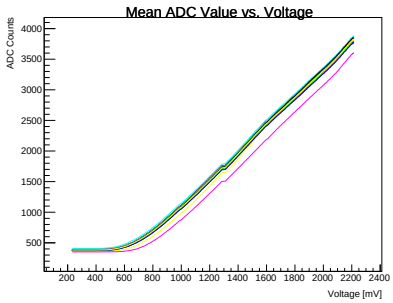

(a) Transfer function for channel 6 (trigger group 2).

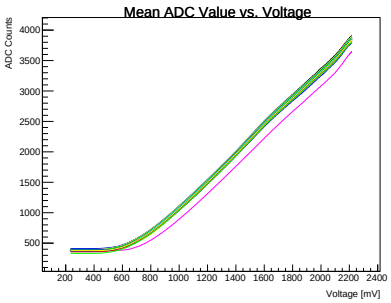

(b) Transfer function for channel 14 (trigger group 4).

Figure 39: Transfer functions for channel 6 and 14 measured by TC.

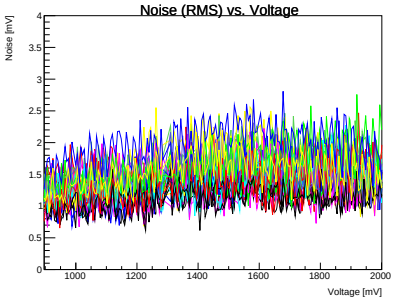

(a) Noise for channel 6 (trigger group 2).

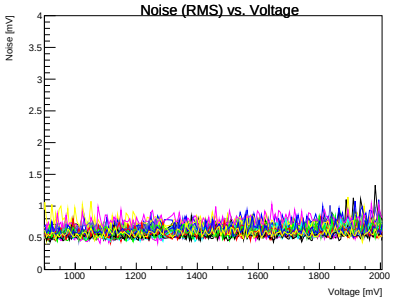

(b) Noise for channel 14 (trigger group 4).

Figure 40: Noise for channel 6 and 14 measured by TC.

A.3 Trigger efficiency measurement

A.3.1 Trigger efficiency - 50 Ω

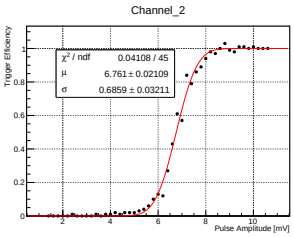

(a) Trigger efficiency for channel 2.

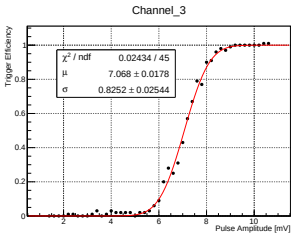

(b) Trigger efficiency for channel 3.

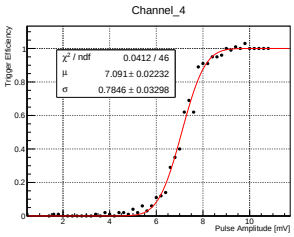

(c) Trigger efficiency for channel 4.

Figure 41: Trigger efficiencies for trigger group 1.

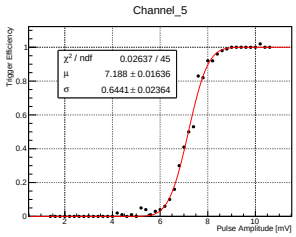

(a) Trigger efficiency for channel 5.

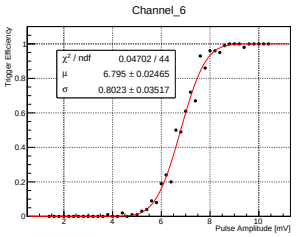

(b) Trigger efficiency for channel 6.

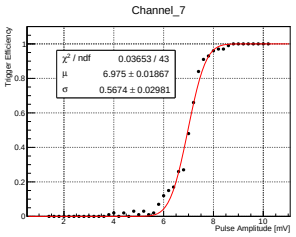

(c) Trigger efficiency for channel 7.

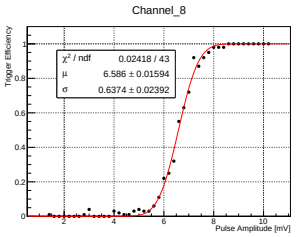

(d) Trigger efficiency for channel 8.

Figure 42: Trigger efficiencies for trigger group 2.

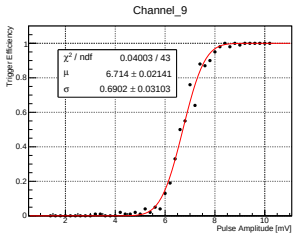

(a) Trigger efficiency for channel 9.

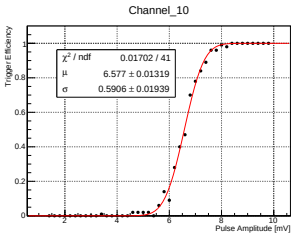

(b) Trigger efficiency for channel 10.

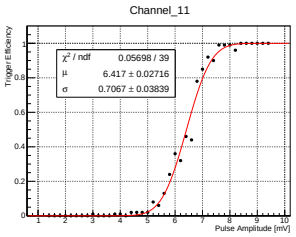

(c) Trigger efficiency for channel 11.

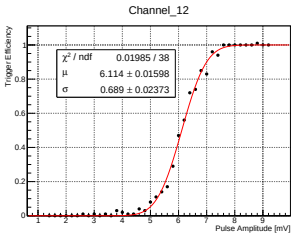

(d) Trigger efficiency for channel 12.

Figure 43: Trigger efficiencies for trigger group 3.

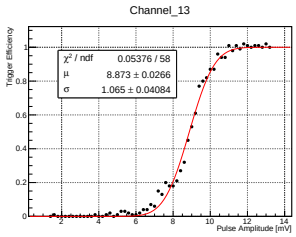

(a) Trigger efficiency for channel 13.

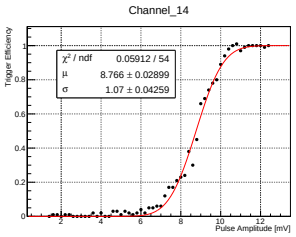

(b) Trigger efficiency for channel 14.

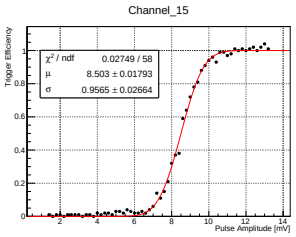

(c) Trigger efficiency for channel 15 .

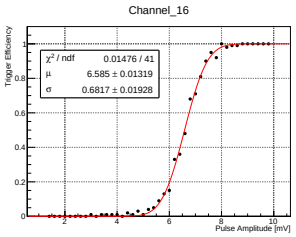

(d) Trigger efficiency for channel 16.

Figure 44: Trigger efficiencies for trigger group 4.

A.3.2 Trigger efficiency - 410 Ω

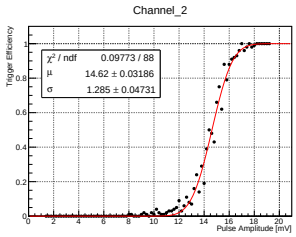

(a) Trigger efficiency for channel 2 with an input impedance of 410 Ω.

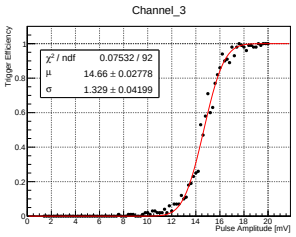

(b) Trigger efficiency for channel 3 with an input impedance of 410 Ω.

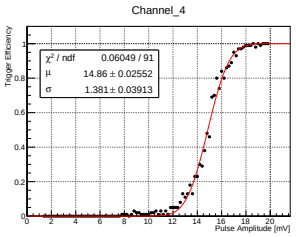

(c) Trigger efficiency for channel 4 with an input impedance of 410 Ω.

Figure 45: Trigger efficiencies for trigger group 1 with an input impedance of 410 Ω.

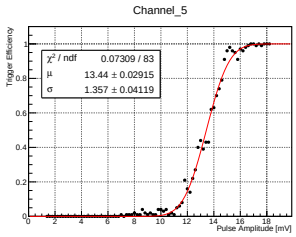

(a) Trigger efficiency for channel 5 with an input impedance of 410 Ω.

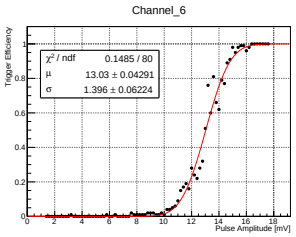

(b) Trigger efficiency for channel 6 with an input impedance of 410 Ω.

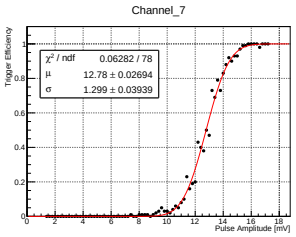

(c) Trigger efficiency for channel 7 with an input impedance of 410 Ω.

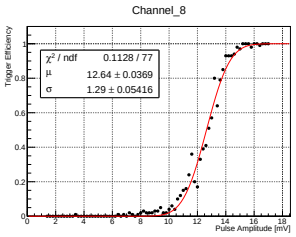

(d) Trigger efficiency for channel 8 with an input impedance of 410 Ω.

Figure 46: Trigger efficiencies for trigger group 2 with an input impedance of 410 Ω.

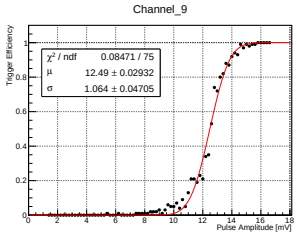

(a) Trigger efficiency for channel 9 with an input impedance of 410 Ω.

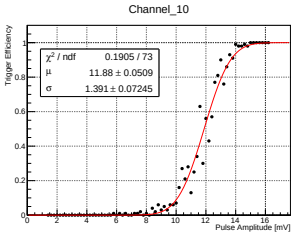

(b) Trigger efficiency for channel 10 with an input impedance of 410 Ω.

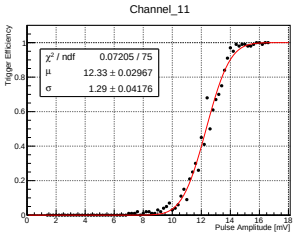

(c) Trigger efficiency for channel 11 with an input impedance of 410 Ω.

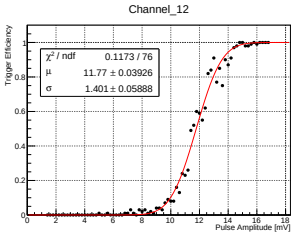

(d) Trigger efficiency for channel 12 with an input impedance of 410 Ω.

Figure 47: Trigger efficiencies for trigger group 3 with an input impedance of 410 Ω.

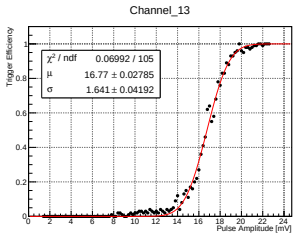

(a) Trigger efficiency for channel 13 with an input impedance of 410 Ω.

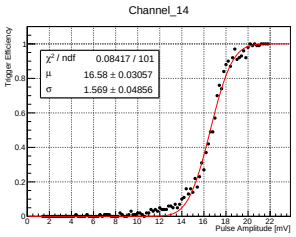

(b) Trigger efficiency for channel 14 with an input impedance of 410 Ω.

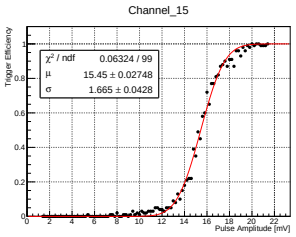

(c) Trigger efficiency for channel 15 with an input impedance of 410 Ω.

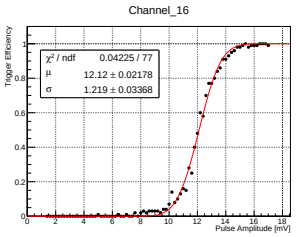

(d) Trigger efficiency for channel 16 with an input impedance of 410 Ω.

Figure 48: Trigger efficiencies for trigger group 4 with an input impedance of 410 Ω.

A.3.3 Parameters

Channel	VPED	TRG_THRES	PMTREF4	WBIAS
2	992	2930	1980	985
3	1005			
4	998			
5	1000	3120	1980	985
6	1009			
7	1001			
8	1023			
9	1000	3170	1980	985
10	1003			
11	1001			
12	983			
13	1000	2770	1980	985
14	993			
15	996			
16	1001			

Table 1: Parameters for the trigger efficiency curves for all channels.

A.4 Threshold versus width measurement

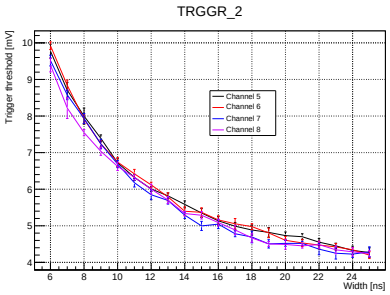

(a) Trigger group 2.

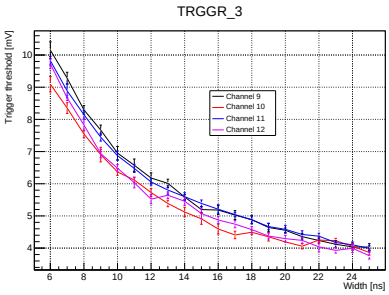

(b) Trigger group 3.

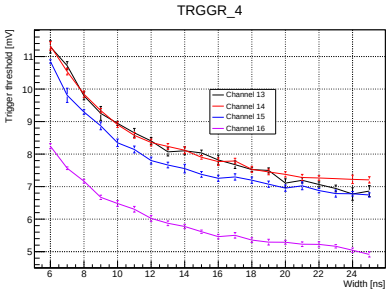

(c) Trigger group 4.

Figure 49: Threshold versus width measurement for different trigger groups.

A.5 Noise versus threshold measurement

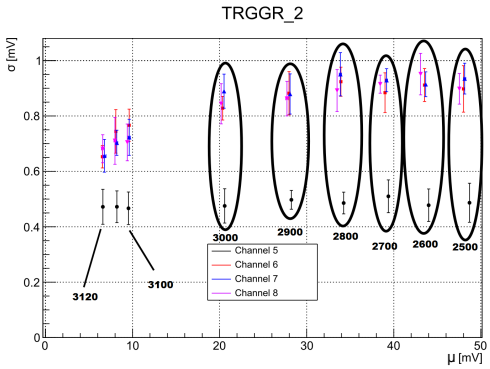

(a) Trigger group 2.

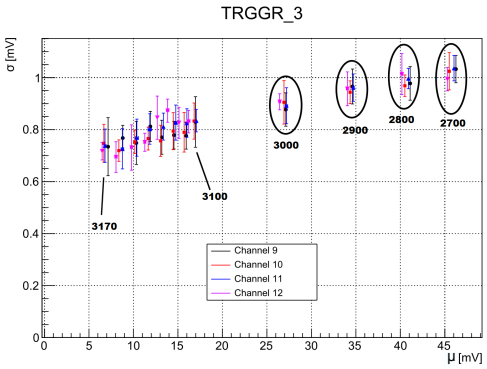

(b) Trigger group 3.

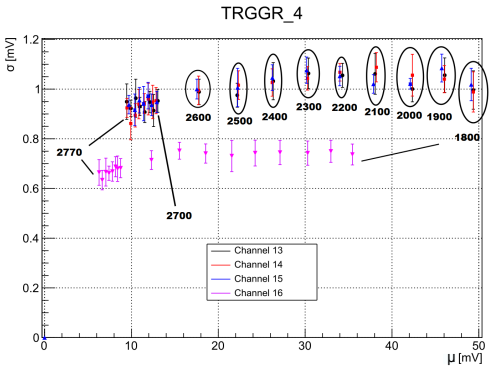

(c) Trigger group 4.

Figure 50: Noise versus threshold measurement for different trigger groups.

References

[1] A. De Franco, R. White. The first GCT camera for the Cherenkov Telescope Array. *In Proceedings of the 34th International Cosmic Ray Conference, ICRC2015*, September 2015.

[2] P. O. Slane B. M. Gaensler. The Evolution and Structure of Pulsar Wind Nebulae. *Astronomy and Astrophysics*, 44:17–47, September 2006.

[3] E. Berger. Short-Duration Gamma-Ray Bursts. *In Proceedings of the 34th International Cosmic Ray Conference, ICRC2015*, September 2015.

[4] H.E.S.S. collaboration. H.E.S.S.-High Energy Stereoscopic System.

[5] A. Albert et al. TARGET 5: a new multi-channel digitizer with triggering capabilities for gamma-ray atmospheric Cherenkov telescopes. *Experimental Astronomy*, 2016.

[6] A.N. Otte et al. Development of a SiPM Camera for a Schwarzschild-Couder Cherenkov Telescope for the Cherenkov Telescope Array. *In Proceedings of the 34th International Cosmic Ray Conference, ICRC2015*, September 2015.

[7] F. Aharonian et al. First detection of a VHE gamma-ray spectral maximum from a cosmic source: HESS discovery of the Vela X nebula, March 2006.

[8] J. Chang et al. An excess of cosmic ray electrons at energies of 300-800GeV. *Nature*, 456:362–365, November 2008.

[9] J. Rousselle et al. Toward the construction of a medium size prototype Schwarzschild-Couder telescope for CTA.

[10] M. Actis et al. Design concepts for the Cherenkov Telescope Array CTA, An Advanced Facility for Ground-Based High-Energy Gamma-Ray Astronomy. *Experimental Astronomy*, 32:193–316, December 2011.

[11] M. Garczarczyk et al. Status of the Medium-Sized Telescope for the Cherenkov Telescope Array. *In Proceedings of the 34th International Cosmic Ray Conference, ICRC2015*, September 2015.

[12] M. Santander et al. Construction of a Medium-Sized Schwarzschild-Couder Telescope for the Cherenkov Telescope Array: Implementation of the Cherenkov-Camera Data Acquisition System. *Annual Review of Astronomy and Astrophysics*, 52:43–105, August 2014.

[13] N. Gehrels et al. A short big gamma-ray burst apparently associated with an elliptical galaxy at redshift z = 0.225. *Nature*, 437:851–854, October 2005.

[14] Pareschi et al. The Layouts of the CTA Array. Unpublished document, 2016.

[15] T. Hassan et al. Layout design studies for medium-sized telescopes within the Cherenkov Telescope Array. *In Proceedings of the 34th International Cosmic Ray Conference, ICRC2015*, August 2015.

[16] G. Häfner, J. Köster. U 05.2 – Faltung einer Gauss-Funktion mit sich selbst.

[17] G. Ghisellini. Gamma Ray Bursts: Basic Facts and Ideas. *International Astronomical Union*, 275:335–343, February 2011.

[18] K. Bernlöhr H. Völk. Imaging very high energy gamma-ray telescopes. *Experimental Astronomy*, 25:173–191, August 2009.

[19] M. Teshima J. Cortina. Status of the Cherenkov Telescope Array's Large Size Telescopes. *In Proceedings of the 34th International Cosmic Ray Conference, ICRC2015*, August 2015.

[20] J. A. Vandenbroucke L. Tibaldo. TARGET: toward a solution for the readout electronics of the Cherenkov Telescope Array. *In Proceedings of the 34th International Cosmic Ray Conference, ICRC2015*, August 2015.

[21] M. S. Longair. *High Energy Astrophysics-Volume 1: Particles, photons and their detection*. Cambridge University Press, Cambridge, 1992.

[22] Technischen Universität München. Cherenkov Telescope Array.

[23] Devon Powell. TARGET 5 Trigger Studies. January 2013.

[24] I. Robson. *Active galactic nuclei*. Wiley, Chichester, 1996.

[25] S. M. Bradbury et al. Detection of γ-rays above 1.5 TeV from MKN 501. *AAP*, 320:L5–L8, April 1997.

[26] T. Greenshaw T. Montaruli, G. Pareschi. The small size telescope projects for the Cherenkov Telescope Array. *In Proceedings of the 34th International Cosmic Ray Conference, ICRC2015*, August 2015.

[27] Luigi Tibaldo. Personal information.

[28] Durham University. Ground Based Gamma Ray Astronomy.

[29] Adrian Zink. Personal information.

Acknowledgements/Danksagung

In diesem kleinen Kapitel möchte ich allen rechtherzlich danken, die zum Gelingen dieser Arbeit beigetragen haben. Besonders bedanken möchte ich mich bei:

- Prof. Dr. Stefan Funk für die Vergabe des spannenden Themas.
- David Jankowsky und Adrian Zink für die klasse Betreuung während der Arbeit und die riesige Geduld, die sie mir entgegenbrachten, sowie das Korrekturlesen.
- Prof. Dr. Gisela Anton für die Übernahme des Zweitgutachtens.
- David Winnekens, Michael Wagenpfeil und Judith Höfer für das Korrekturlesen und den hilfreichen Tipps.
- Bei der gesamten CTA Arbeitsgruppe für die herzliche Aufnahme und die witzigen Mensagespräche.
- Meinem Freund, Emanuel Freundl, für die Unterstützung während meines bisherigen Studiums, besonders während der stressigen Klausurphasen, sowie während dieser Arbeit.
- Meiner ganzen Familie für die Unterstützung bei allem was mir in den Kopf kommt und besonders möchte ich mich bei meiner Mama bedanken für das ständige Vorrantreiben, ohne dich wäre ich niemals soweit kommen.

DANKE!

Eidesstattliche Erklärung

Ich versichere hiermit an Eides statt, dass ich die vorliegende Bachelorarbeit mit dem Titel “Characterization of a custom designed trigger ASIC (T5TEA) for the Cherenkov Telescope Array” selbstständig und ohne unzulässige fremde Hilfe erbracht habe. Ich habe keine anderen als die angegebenen Quellen und Hilfsmittel benutzt sowie wörtliche und sinngemäße Zitate kenntlich gemacht. Die Arbeit hat in gleicher oder ähnlicher Form noch keiner Prüfungsbehörde vorgelegen.

Datum, Ort

Unterschrift